Volume 27
Number 43
21 November 2025
Pages 13517-13956

Green Chemistry

Cutting-edge research for a greener sustainable future

rsc.li/greenchem

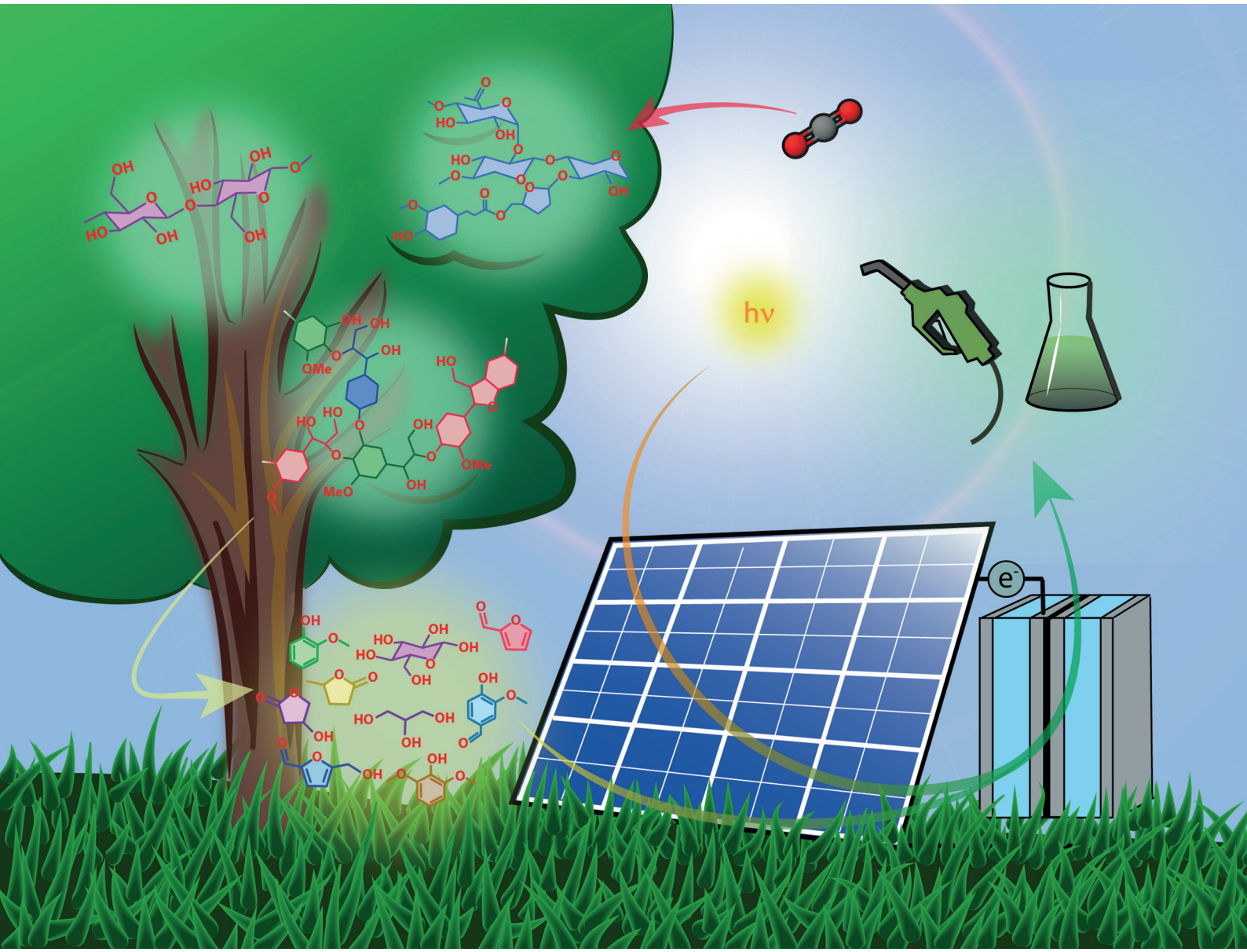

ISSN 1463-9262

ROYAL SOCIETY OF CHEMISTRY

CRITICAL REVIEW

Mathieu S. Prévot *et al.*

Powering lignocellulose biorefineries with solar energy – a critical review with furfural as a case study

25 YEARS ANNIVERSARY

Green Chemistry

CRITICAL REVIEW

View Article Online
View Journal | View Issue

Cite this: *Green Chem.*, 2025, **27**, 13529

Powering lignocellulose biorefineries with solar energy – a critical review with furfural as a case study†

Clément Spadetto, Cyril Hachemi and Mathieu S. Prévot *

In the context of a circular carbon economy, biorefineries are set to replace traditional petrochemical installations. While a standard biorefinery model involves the use of decarbonized electricity and reactive gases (such as H_2 from electrocatalytic water splitting) to process and upgrade biomass resources, more integrated approaches can be envisioned. In particular, the direct use of solar energy and water as a source of protons in solar-powered electrolysers and photoelectrocatalytic and photocatalytic devices appears attractive. However, the range of chemical transformations accessible through thermocatalytic, electrocatalytic or photocatalytic processes varies greatly, and so do the corresponding operating conditions. Therefore, it is still unclear whether integrating solar strategies into biorefineries would be energetically and economically efficient. In this critical review, we provide elements to address this outstanding question for lignocellulose biorefineries. First, we present a comparative overview of the current state-of-the-art of catalytic processes for lignocellulose valorisation by thermochemical, electrochemical and photoelectrochemical/photochemical approaches, along with their required energy input and operating conditions. Then, we propose a case study on lignocellulose-derived furfural hydrogenation, in which we evaluate the opportunity of replacing established thermocatalytic processes with solar-powered electrochemical processes. We show that there exists a range of conditions in which it is more beneficial to transform furfural electrochemically, and that expanding these considerations to other biomass valorization processes would be useful. Finally, we describe how including integrated solar-powered chemical transformation into biorefinery plants unlocks novel strategies and synergies for future biorefinery designs. Overall, we conclude that there is an interest in supplying solar energy and electrons directly to the catalytic transformations, provided that dedicated and specific catalysts and processes are developed for this purpose.

Received 24th March 2025,
Accepted 15th July 2025

DOI: 10.1039/d5gc01462j

rsc.li/greenchem

Green foundation

1. This critical review discusses whether introducing solar-driven approaches in lignocellulose biorefineries can help lower their energy and carbon intensity, in the context of a circular use of carbon resources.
2. As one of the major consumers of fossil energy and feedstocks, the chemical industry needs to undergo an important shift towards circular models. The approaches discussed in this critical review are of interest for the defossilization of a wide array of chemical processes, from fuel production to commodity and specialty chemical production.
3. We show that, under the right conditions, solar-powered electrolysers can improve both the energy intensity and carbon emission balance of a lignocellulose biorefinery on an industrial scale. Our work highlights and demonstrates the benefits of progressing scientific research around these emerging technologies (electrocatalysis, photoelectrocatalysis) to improve the sustainability of lignocellulose refineries in the short and long-term.

1. Introduction

Modern societies are fully dependent on a large array of carbon-based chemicals, including fuels, plastic materials, or pharmaceuticals. Their current industrial production overwhelmingly relies on fossil resources, used both as feedstock and an energy source. While this fossil-fuelled petrochemical industry has successfully supplied the world with crucial

Université Claude Bernard-Lyon 1, CNRS, IRCELYON, UMR 5256, Villeurbanne F-69100, France. E-mail: mathieu.prevot@ircelyon.univ-lyon1.fr

†Electronic supplementary information (ESI) available: List of equations and parameters used in the techno-economic modelling. See DOI: https://doi.org/10.1039/d5gc01462j

chemicals for the past decades, it is also currently one of the main contributors to ever-increasing levels of atmospheric CO_2. As such, it is directly responsible for deleterious effects on the climate, and ultimately human populations, on a global scale. Thus, a shift away from this model and the implementation of carbon-neutral alternatives – the so-called "defossilization" of the chemical industry – is urgently needed. However, a systemic change of this magnitude is certainly a tall order and will likely only be achieved through the deployment of complementary, location-dependent, technological approaches on different scales, and with different levels of integration. One appealing approach consists of advancing solar-driven biorefineries, *i.e.* structures powered by carbon-free electricity in which feedstocks composed of contemporary carbon are converted to value-added commodity chemicals in a circular fashion. In this context, the largest reservoir of renewable complex carbon-based molecules is the biomass, and it has therefore naturally been considered as a prime feedstock for biorefineries. While initial efforts, in particular for the production of defossilized biofuels, have focused on using vegetable oils and sugars, they were and still are in direct competition with the production of crops for food production. This raises ethical concerns and is also likely to worsen the transgression of the planetary boundary on land use change.[1,2] More recent developments instead focus on the valorisation of the non-edible part of biomass, consisting primarily of lignocellulosic biomass waste or algae.[3,4] Lignocellulosic biomass can itself be divided into three main polymeric chemical components: lignin, cellulose and hemicellulose. Together they exhibit a rich chemistry through phenolic units (in lignin), C6 sugar units (in cellulose and hemicellulose) and C5 sugar units (in hemicellulose), which can be processed in dedicated infrastructures. Corresponding lignocellulosic biorefinery models typically include two sequential processes: (i) a pre-treatment or primary refining to separate lignin, cellulose and hemicellulose and (ii) a secondary refining, involving a range of catalysed reactions to break down, upgrade and functionalize these three polymeric substrates and generate value-added chemicals.[5] Currently, the processes used in this secondary refining take inspiration from the long-established catalytic petrochemical refining industry, and often involve heating under pressure of reactive gases (O_2, H_2) and/or liquid (alkaline or acidic water, organic solvents). While it is possible to drive them with carbon-free electricity through resistive heating and electric compressors, and to employ decarbonized reactive gases (*e.g.* obtained through water electrolysis or separated from the air by pressure swing adsorption), there is also an opportunity to directly use these "green" electrons to perform some of these processes electrochemically. Thus, developing electrocatalytic biorefinery models presents the double advantage of removing energy conversion systems (electricity-to-heat, electricity-to-pressure) from the balance of plant, and directly using water under ambient conditions rather than pressurized reactive gases as a source of oxygen atoms and protons to perform redox transformations. Finally, one additional level of integration for solar biorefineries would consist of directly powering chemical transformations with solar photons in photocatalytic or photoelectrocatalytic reactors. While all these integrated solar-to-chemical approaches, illustrated in Fig. 1, could in principle lead to an improved per-

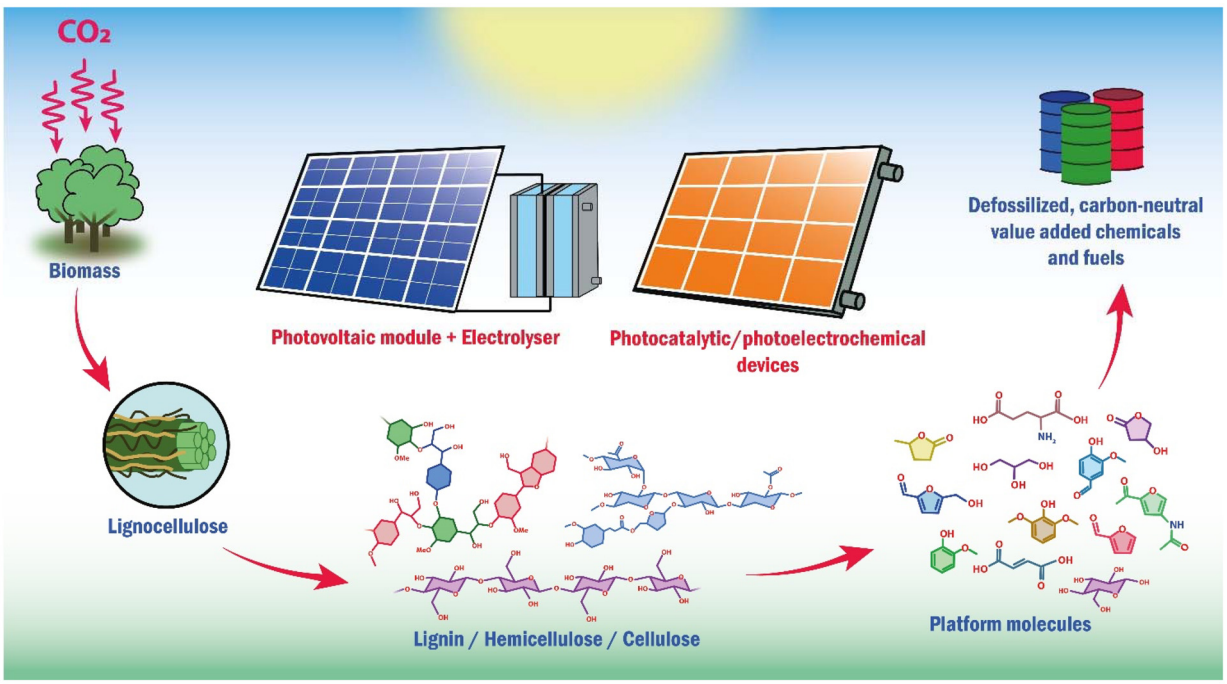

Fig. 1 Illustration of the general value-chain of carbon-based chemicals involved in lignocellulose valorisation and solar-to-chemical technological solutions available to carry them out inside solar biorefineries.

formance and reduced footprint for solar biorefineries, their development currently remains in its early stages, and there is a lot of uncertainty over the required conditions necessary for their practical and competitive implementation compared with more mature technologies. This critical review, in addition to providing a snapshot of the current state-of-the-art in solar-to-chemical approaches for the valorisation of lignocellulose, aims at proposing relevant lines of reflection on the basis of a concrete case study around furfural, a major bio-based chemical already produced on an industrial scale. Here, we aim to provide a valuable contribution to the development of the rapidly expanding field of investigation into solar biorefineries and the defossilization of the chemical industry at large.

2. Solar-to-chemical approaches in biorefineries

As briefly mentioned in the introduction, there are several ways to power chemical transformations in biorefineries by sunlight, with different levels of technological integration (see Fig. 2). In the particular case of lignocellulose, its activation and conversion are notably difficult because of (i) the sturdiness and low chemical reactivity of lignin that hinder the reactive availability of cellulose and (ii) the crystallinity of cellulose domains themselves, which grants them a high resilience towards hydrolysis. Therefore, an initial fractionation step is required: lignin, cellulose and hemicellulose are typically separated by a preliminary chemical treatment in appropriate solvents, such as a combination of concentrated acid and acetone or ethanol,[6,7] or more recently in ionic liquids or deep eutectic solvents,[8–10] followed by separation and purification steps.

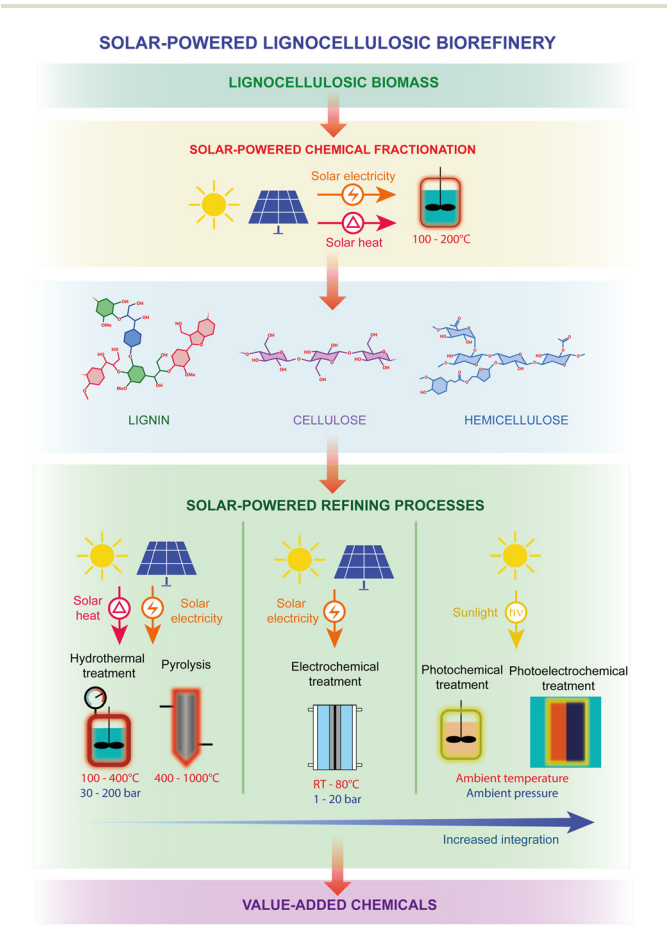

Fig. 2 Illustration of possible approaches to implement solar-powered processes in lignocellulose biorefineries for the production of value-added chemicals from raw biomass.

Alternatively, approaches involving bacterial or enzymatic processing are also developed to activate lignocellulose.[11,12] Inside a solar biorefinery, it is easily conceivable to provide the energy required for these treatments under mild conditions of temperature and pressure through solar heat and electricity. At the outset of this fractionation step, lignin, hemicellulose and cellulose can be processed independently for further valorisation inside the plant.

2.1 Thermocatalytic processes powered by solar electricity

The simplest approach for the upgrading of pre-treated lignocellulose fractions, with a minimal degree of integration, consists of carrying out thermocatalytic reactions in reactors powered by renewable solar electricity (or potentially directly by solar heating). A large number of excellent reviews are available on recent progress achieved in the very active field of thermocatalytic lignocellulose valorisation, the details of which will not be extensively covered in this manuscript.[5,13–21] Instead, we provide an overview of representative processes and the conditions of temperature and pressure they require. Fig. 3a summarizes the ranges of pressures and temperatures involved in typical biomass treatment processes. Importantly, specific and distinct value chains can be derived from each component of lignocellulose (lignin, cellulose, hemicellulose) in a biorefinery. A (non-exhaustive) selection of the corresponding transformations is provided on Fig. 3b–d, and the associated processes are discussed in the following section.

2.1.1 Lignin conversion. A wide range of thermochemical techniques have been developed to break down and valorise lignin. Typically, a primary treatment is conducted to generate small oligomers (generally under the form of a bio-oil). This difficult transformation requires relatively harsh conditions in terms of temperature, pressure or chemical reactivity and is usually performed either by pyrolysis or hydrothermal treatments (carbonization, liquefaction or gasification). This step generates bio-oils with a high percentage of oxygen atoms (typically above 30 wt%), which causes them to be more unstable and more corrosive than their fossil counterparts, mainly composed of less-reactive carbon–carbon and carbon–hydrogen bonds. For this reason, a second step of deoxygenation is required to stabilize bio-oils before their conversion to value-added chemicals. The most common process to perform this stabilization is termed hydrodeoxygenation (HDO) and consists of heating raw bio-oil (at 200–400 °C) under H_2 pressure (50–200 bars) in the presence of heterogeneous (often bifunctional) catalysts.[22,23] The bio-oil obtained after the HDO

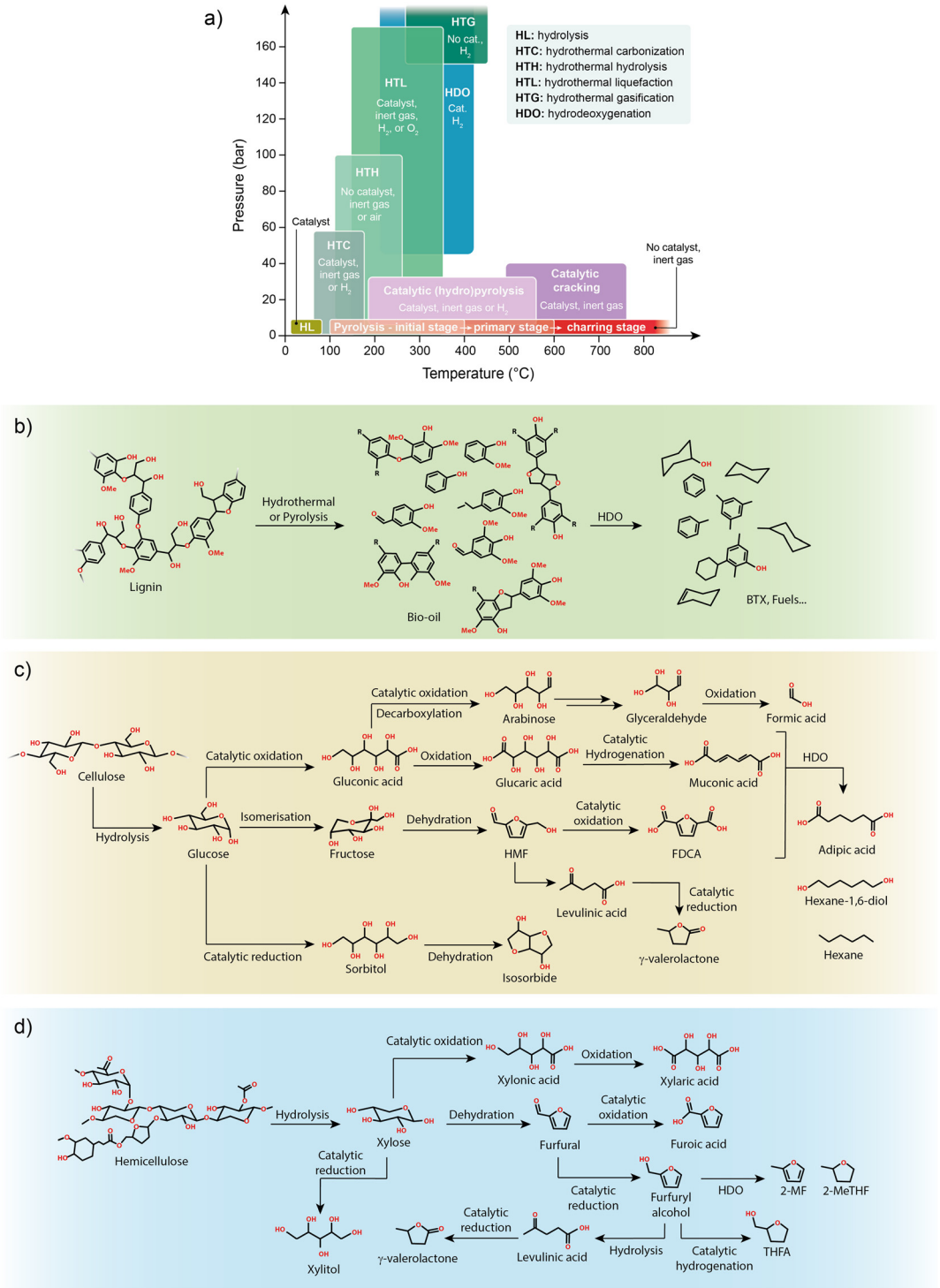

Fig. 3 (a) Selection of thermochemical processes integrated in lignocellulose biorefineries organized as a function of their operating temperature and pressure ranges. Illustration of possible associated value chains for lignin (b), cellulose (c) and hemicellulose (d). BTX = benzene, toluene, xylene; 2-MF = 2-methylfuran; 2-MeTHF = 2-methyltetrahydrofuran; THFA = tetrahydrofurfuryl alcohol.

step typically contains 70–100% less oxygen than initially, and can be further processed for use in the energy or chemical industries. This stabilized bio-oil still contains a wide range of (mostly cyclic) aromatic and aliphatic compounds with varied molecular weights. Smaller aromatic compounds, labelled as BTX (for benzene–toluene–xylene), can be used as high-

tonnage feedstock for the chemical industry, while cyclic aliphatic compounds (cyclohexane and its derivatives) are typically used as solvents or primary reagents on an industrial scale. Moreover, lignin-derived bio-oil is also considered as an attractive feedstock for the development of sustainable aviation fuels (SAF). However, obtaining the ideal aromatic/aliphatic ratio in the oil composition, complying with the physicochemical requirements of jet engines, remains a challenge. Overall, despite outstanding challenges, lignin is considered as a promising biomass feedstock to specifically replace the petrochemical naphtha and its value chain in biorefineries.

2.1.2 Cellulose and hemicellulose conversion. The main conversion pathway of cellulose consists of conducting its hydrolysis, catalysed in acidic solution or on the acidic surface of a heterogeneous catalyst. This is performed at ambient or mild temperatures (25–150 °C) and results in the formation of sugars (glucose, arabinose, xylose, *etc.*). Glucose (the main product of cellulose hydrolysis) can be transformed to sorbitol under hydrogenation conditions, at the surface of Ru or Ni catalysts.[24] While nickel presents the advantage of lower cost and lower criticality, it has been reported to undergo leaching under hydrogenation conditions, leading to catalyst deactivation and additional product purification. Moreover, glucose hydrogenation requires high pressures of H_2 (40–80 bars). To address these shortcomings, recent works have focused on transfer hydrogenation strategies with increasing success.[25–27] Another value chain involves the isomerization of glucose to fructose in the presence of a Lewis acid (*e.g.* Sn-doped or NaX zeolites, hydrotalcites).[24] The main limitations of this process are its endothermicity ($\Delta H \sim 3$ kJ mol^{-1}) and reversibility ($K \sim 1$ at 25 °C), requiring efficient equilibrium displacement to reach high conversion yields. Fructose can itself be decomposed into dihydroxyacetone (DHA) and glyceraldehyde through a retro-aldol process in the presence of a Lewis acid, *en route* to lactic acid. Fructose can also be dehydrated under Brønsted acidic conditions to generate 5-hydroxymethylfurfural (HMF).[24,28] This can be done homogeneously using inorganic or organic acid catalysts or metal chlorides. This can also be performed heterogeneously at the surface of zeolites, metal phosphates, metal–organic frameworks or functionalized silica. Considering the need for both types of acidity, heterogeneous catalysts exhibiting both Lewis and Brønsted acidic sites are increasingly under scrutiny to perform the one-pot conversion of glucose to HMF.[29–31] However, an advanced mechanistic understanding of fructose conversion at these Brønsted and Lewis acidic sites is still required to fine-tune and optimize the selectivity towards HMF or DHA/lactic acid. Additionally, the use of biphasic solvent systems has proved useful in HMF synthesis, as it helps in shifting the equilibrium towards the product.[32–35] Finally, the oxygenated products resulting from the aforementioned processes can themselves be further converted to C6 cyclic ethers, *n*-hexanol, 2-hexanone or hexane by regular HDO.

Glucose can alternatively be oxidatively converted to gluconic or glucaric acid. The production of gluconic acid is typically performed with supported Pt, Pd or Au, on TiO_2 or carbon, in alkaline conditions, and under low pressure of O_2 or air (1–5 bars).[24,36–38] While non-noble metal alternative are under investigation, no convincing candidate has shown promise for a scaled-up process, and Au remains the best trade-off between activity, stability and cost to date. Glucaric acid can be obtained with Pt-based catalysts in neutral or alkaline conditions, but at higher O_2 pressures (above 10 bars) and temperatures (80–100 °C).[36–39] Moreover, selectivity for glucaric acid remains low, due to the high number of side processes that the intermediate can undergo, typically leading to C–C cleavage events and resulting in the production of smaller carboxylic acids.

On the other hand, HMF can be oxidized to furandicarboxylic acid (FDCA), a bioplastic precursor. Again here, Pt, Pd, Ru and Au are the most efficient catalyst to perform this process with O_2 as the oxidant (1–10 bars), under mild temperatures and in alkaline conditions. Supporting nanoparticles of these metals on oxide supports has proved to be a successful approach to reach complete selectivity towards FDCA. We direct the reader to a number of recent reviews detailing catalytic approaches for these processes.[24,36,40–43]

While the value chain of cellulose is centred on C6 sugar conversion, the hydrolysis of hemicellulose similarly allows access to C5 sugar chemistry *via* the xylose molecule. The main valorisation pathway for xylose currently consists of dehydrating it into furfural in the presence of Lewis and Brønsted acid catalysts, such as acidic zeolites or char impregnated with metal chlorides. This is already deployed on an industrial scale through the Quaker Oats, Agrifuran, Petrole-Chimie Escher Wyss or Rosenlew processes.[44] Furfural can then be upgraded into furfuryl alcohol (a component of industrial binders and glues), 2-methylfuran or tetrahydrofurans (potential biofuel additives, biofuel precursors or even drop-in biofuels, as well as green solvents)[45–47] under controlled HDO conditions. The hydrogenation reaction towards furfuryl alcohol is usually performed with noble metal catalysts (Pt, Pd, Ru), often supported on metal oxides, or alternatively on Cu, Co or Ni oxide surfaces, inside an alcohol solvent, around 10 bars of H_2 and below 120 °C.[44,48] Using the same catalysts and increasing the pressure of H_2 above 10 bars usually allows access to more reduced tetrahydrofurans. Finally, 2-methylfuran is usually obtained at higher temperature (above 200 °C) and above 10 bars of H_2 (or using small alcohols as hydrogen donors in transfer hydrogenation schemes). Typical catalysts are again carbon- or oxide-supported noble metals (Pt, Ru, Pd) or Cu- or Ni-based materials.[44,49,50] Furfural can alternatively be oxidatively converted to furoic acid, a precious platform for the synthesis of fine chemicals.[51] This is usually performed on Au-based catalysts, although transition metals such as Cu and Mn have recently been explored. Finally, as with glucose, xylose can be reduced to xylitol (a sweetener used in the food industry) or oxidized to xylonic or xylaric acid (a bioplastic precursor). Finally, both HMF and furfural can be catalytically be broken down into formic acid and levulinic acid. This is once again performed in reductive conditions, with a combination of Lewis and Brønsted acid sites.[36] The former catalyses the

hydrogenation of the furan ring, while the latter catalyses the hydrolysis and ring-opening leading to the final product. Using bifunctional Lewis and Brønsted acidic catalysts, and isopropanol as a hydrogen donor (instead of high pressures or H_2), allows access to γ-valerolactone from levulinic acid (or directly from HMF or furfural in a one-pot fashion), a non-toxic chemical with applications as bio-fuel component, lubricant, or green solvent.

Overall, the conversion of cellulose and hemicellulose mainly involves Lewis and Brønsted acidic catalysts, in liquid media, under pressure of reactive O_2 or H_2 (with the exception of transfer hydrogenation approaches). The use of noble metals in hydrogenation reactions also remains the standard, despite the more recent development of transition metal alternatives. Still, these processes tend to be driven in much milder conditions than the lignin conversion described in the previous section.

In summary, the different thermal or thermocatalytic processes involved in the conversion of lignocellulose to valuable chemicals and fuels involve temperatures in the 100–1000 °C range (can be lowered to 150–600 °C if the charring stage of pyrolysis is excluded) and high pressures of reactive O_2 or H_2 gas (in particular in the HDO steps). Additionally, the use of critical materials and/or organic solvents is often required. Thus, to conduct these processes in a carbon-neutral fashion it is necessary to use electrical ovens running on renewable electricity or to drive the processes photothermally. In fact, recent progress on the latter approach showed promise for synergistic integration in solar biorefinery.[52] However, despite the manifest interest in this approach, the relatively low amount of literature available as of now on the topic makes it difficult to assess compared with other technologies. Moreover, operating carbon-neutral reduction processes implies either relying on natural H_2 sources (whose unclear abundance and/or dilution currently hinders its reliability for the needs of the chemical industry) or producing it from water by means of solar-powered electrolysers, which is the preferred strategy in most energy transition roadmaps. However, directly driving the conversion of biomass resources through electrocatalytic processes offers interesting alternative, complementary or potentially more efficient pathways to generate target value-added molecules.

2.2 Electrocatalytic processes powered by solar electricity

An attractive alternative to defossilizing thermocatalytic high-temperature, high-pressure processes is to drive these processes electrocatalytically instead. In contrast to thermally-driven redox transformations, involving O_2 or H_2 gas as oxidant or reductive reagent, respectively, electrochemical reactions proceed through concerted or sequential exchanges of protons (with the typically aqueous media) and electrons (with the electrode). Regarding reduction processes, two main mechanisms are observed:

(i) *Electrochemical hydrogenation (ECH)*: the adsorbed organic substrate chemically reacts with adsorbed hydrogen atoms (H*) produced through a Volmer step ($H^+ + e^- \rightarrow H^*$).

(ii) *Proton-coupled electron transfer (PCET)*: a proton from the solution and an electron from the electrode are simultaneously transferred to the adsorbed organic substrate.

Similarly, oxidation processes can proceed through one of two pathways:

(i) *Electrochemical dehydrogenation or indirect oxidation*: the electrocatalyst surface is first oxidized (and releases a proton or a molecule of water to the electrolyte and an electron to the electrode), and subsequently oxidizes the adsorbed organic substrate while returning to its initial oxidation stage.

(ii) *Proton-coupled electron transfer (PCET) or direct oxidation (see above).*

These processes are very efficient at forming or breaking C–H or C–O bonds under standard electrochemical conditions. Moreover, while the formation of C–C bonds and oligomerization can also be easily accessed (especially at high concentrations in organic substrate), the breaking of C–C bonds in the polymer backbone is more challenging in the mild conditions of temperature (below 100 °C) and pressure (1–10 bars) encountered in conventional electrolysers. For these reasons, to date, most efforts have been focused on the valorisation of small platform compounds found in pyrolytic or hydrothermal bio-oils (phenolic molecules, alcohols, carboxylic acids) or hydrolysis products (sugars and furanic compounds) rather than on the direct valorisation of lignocellulose or its primary polymeric components.

2.2.1 Reduction processes. As mentioned in the previous section, there is a strong interest in removing oxygen atoms from compounds in lignocellulosic bio-oils, so as to improve their chemical stability and processability. Therefore, a lot of effort has been devoted to the development and optimization of reduction electrocatalysts for biomass valorisation. For instance, the electrochemical reduction of furfural has been extensively studied on copper surfaces, where three main products can be obtained: furfuryl alcohol, 2-methylfuran and hydrofuroin, resulting from the reductive coupling of two furfural molecules.[53–70] The selectivity of the process is strongly affected by the pH of the electrolyte, the concentration of furfural and, to a lesser extent, the counterions present in the electrolyte. Indeed, it was reported that furfural can be selectively converted to furfuryl alcohol in dilute neutral and alkaline conditions, while it is preferentially converted to 2-methylfuran under acidic conditions (albeit with a stronger competition from the hydrogen evolution reaction). Glucose reduction into sorbitol has also been performed electrocatalytically,[71,72] but only with moderate faradaic efficiencies (FE), peaking at 57% at the surface of Zn–Fe in mildly alkaline electrolyte (pH 11).[73] The process has further been studied in mildly acidic to mildly alkaline conditions at the surface of Zn-,[74,75] Ni-,[76] and Pb-based[74,77,78] electrodes, with FE in the 15–40% range. Alternatively, the reduction of small lignin-derived phenolic compounds (phenol, guaiacol, catechol, cresol) was also performed in electrochemical reactors, typically using Ni-, Pd-, Pt-, or Rh-based cathodes in acidic conditions.[79,80] While the hydrogenation of the aromatic ring was reliably and successfully achieved under cathodic bias, the hydrogenolysis of the methoxy or phenol moieties was hardly

observed under electrochemical conditions (as opposed to thermochemical HDO where hydrogenolysis can be selectively performed to generate BTX compounds). Moreover, in the reports available to date, the electrochemical hydrogenation of phenolic compounds usually proceeds through an indirect mechanism, where the limiting step (H transfer to the organic substrate) is chemical in nature and therefore insensitive to potential bias. Unfortunately, this strongly limits the advantage of using electrocatalytic processes compared with thermocatalytic HDO, since the catalytic mechanism is effectively limited by the same elementary step. Another reduction process under investigation for biomass valorisation is the conversion of levulinic acid to valeric acid. Indeed, valeric acid has been identified as a possible intermediate *en route* to so-called "valeric biofuels", essentially composed of valeric esters.[81] It is currently produced industrially through the hydroformylation of fossil-based 1-butylene, while its synthesis from biomass-derived levulinic acid involves several catalytic steps: dehydration of levulinic acid to γ-valerolactone, ring opening to 3-pentanoic acid, and hydrogenation to valeric acid. While all these steps can be performed in one pot, the process relies on high temperatures and pressures, and precious metal catalysts (*e.g.* Pt, Ru, Pd) prone to deactivation through coking. In this context, electrocatalysis offers an attractive alternative: levulinic acid can be converted selectively to valeric acid at the surface of Pb, Cd, Zn or In electrodes in acidic conditions.[82,83] It is clear that some reduction products (mainly hydrogenated aromatic rings) remain practically inaccessible through electrocatalysis so far, thereby restricting the deployment of the technology to a smaller scope of products. Still, the use of water as a hydrogen donor and a generally easier use of transition metals under stable conditions compared with the thermocatalytic processes discussed in the previous section, justifies investigating electrocatalytic pathways in the context of green chemistry. For all the reduction processes outlined in this section, substituting traditional thermal catalysis by electrocatalytic processes offers the common advantages of avoiding high pressures of H_2, high temperature and catalyst deactivation through coking, while offering good selectivity for the value-added products. However, the competitiveness of electrocatalysis compared with thermal catalysis remains to be established through energy efficiency and cost comparisons, as well as durability measurements which are scarcely performed and reported in the literature. We address part of this knowledge gap in section 3.

2.2.2 Oxidation processes. While less relevant for the production of energy carriers, the electrocatalytic oxidation of biomass-derived chemicals has the potential to simultaneously generate value-added chemicals as feedstocks for the chemical industry and lower the energetic cost of electrolysis by replacing the ubiquitous water oxidation to oxygen balancing the majority of reduction processes in aqueous media. In recent years, the electrocatalytic oxidation of HMF to FDCA has known a rapid surge in interest and is currently the object of very active global investigation work. FDCA has been identified as a promising replacement for the terephthalic acid monomer in polyethylene terephthalate, a plastic material extensively used in packaging. The biomass-based polymer produced from FDCA and ethylene glycol, polyethylene furoate, has indeed shown satisfying mechanical and chemical properties as a replacement.[84,85] Taking inspiration from alkaline water oxidation anodes, Ni-based materials have been shown to catalyse the indirect electrochemical oxidation of HMF to FDCA with 100% selectivity at high pH.[86–99] However, this technology faces some limitations, as the generation of Ni(III)OOH species from Ni(II) at the surface of the electrode is required to trigger the oxidation of HMF (indirect oxidation pathway) and only occurs at potentials more than 1 V higher than the standard oxidation potential of HMF (estimated around +0.3 V *vs.* RHE).[100,101] This results in important overpotentials and thus energy losses in the process. Ni has been combined with other metals (Co, Cu, Cr and Fe) to improve its activity or in an attempt to shift the onset of catalytic oxidation towards more cathodic potentials, but only with moderate success.[102] Other anode materials have been employed for HMF oxidation in basic pH, including Au,[103] Au–Pd,[104–106] Co,[107–110] Pt,[111] and Mo.[112] Moreover, the electrochemical oxidation of HMF has also been studied at lower pH on Au-,[113] Pd-, Ru-,[114,115] and Mn-containing[116,117] anodes. In summary, FDCA can be selectively obtained at the surface of Ni, Co, Mn and Mo at room temperature at a similar range of (relatively high) operating oxidation potentials. On the other hand, Au, Pt, Pd and Ru can convert HMF at much lower potentials, but at the expense of selectivity, as diformylfuran (DFF), 5-hydroxymethyl-2-furoic acid (HMFCA), and 5-formyl-2-furoic acid (FFCA) are also obtained in high quantities. Interestingly though, the selectivity can be better directed towards FDCA by alloying metals (Au–Pd)[104] or raising the temperature of the reactor.[115] Moderate heating also helps to improve the solubility of FDCA at low pH, which can then be easily recovered by recrystallization at ambient or lower temperature. Still, an important challenge of performing oxidation processes at low pH is to make sure that the electrodes are chemically resilient to the operating conditions and do not leach into the electrolyte over time. So far, little can be found in the literature on this front for acidic/neutral electrochemical HMF oxidation.

Another valorisation pathway accessible electrochemically consists of directly oxidizing glucose, and converting it to gluconic or glucaric acid, or arabinose. These products have significant economic value for applications in the cosmetics and pharmaceutical industries, but their market remains relatively small compared with commodity chemicals like fuels and plastics. Thus, for larger scale development, it is also possible to target the conversion and breakdown of glucose to formic acid, a potential energy carrier for emerging fuel cell technologies. The electrocatalytic oxidation of glucose is typically performed in alkaline conditions on Pt-,[118,119] Pd-,[119,120] Au-,[119,121,122] Mn-,[123] or Ni-based[122,124–126] anodes. Interestingly, glucose can be oxidized at lower potentials than HMF,[127] resulting in lower energy requirements. This can be leveraged to improve the efficiency of an electrochemical process generating a valuable reduction product at the corresponding

cathode. In this case, the complete oxidation of glucose to CO_2 at the anode can also be considered as a "clean" way to lower the working voltage of an electrolyser where only the reduction product stays in the liquid phase. Similarly, xylose obtained from hemicellulose can be oxidized to xylonic, xylaric or formic acid, or all the way to CO_2 on the same anodes. However, one important drawback of electrochemical polyol oxidation is the tendency of some intermediates (acyl, carbonyl) to poison the surface of the electrode, thus necessitating the inclusion of frequent anode regeneration steps in the process.[119,128]

Finally, the electrochemical oxidation of lignin monomers and oligomers, or even actual lignin, has also been investigated.[129,130] As the most common linkage in lignin is the β-O-4 linkage, model compounds exhibiting this linkage have been subjected to electrochemical oxidation in several conditions. Using redox mediators such as 2,2,6,6-tetramethyl-1-piperidine *N*-oxyl (TEMPO) or 4-acetamido-TEMPO (ACT), the β-O-4 linkage can be oxidized to a carboxylate moiety in basic conditions at the surface of a glassy carbon electrode,[131] or in the absence of a mediator at the surface of PtRu-[132] or carbon-based[133] electrodes. This carboxylation can be leveraged to further break the linkage and initiate lignin depolymerization under acidic conditions. It is also possible to effect the oxidative breaking of β-O-4 linkage in a sequential process involving an electrocatalytic oxidation followed by a photocatalytic cleavage involving an Ir complex in organic medium.[134] Unfortunately, the use of redox mediators in organic solvents suffers from chemical mediator degradation over time and is unlikely to be easily scalable. Regarding more practical applications, the electrocatalytic oxidation of lignin has been investigated as early as 1946 on a Pb anode in sodium hydroxide.[135] Since then, alkaline electrolytes have mostly been favoured as they can result in (partial) depolymerization of lignin. Anodes in PbO_2,[136–139] IrO_2,[140] NiSn,[141] Pt–Ru[142] or the more complex Ti/SnO_2-Sb_2O_3/PbO_2[143] have been evaluated for this purpose. Overall, all these electrodes allow the depolymerization of a fraction of the lignin and its conversion to valuable chemicals such as vanillin, phenolic oligomers or small carboxylic acids. Still, selectivity remains an important issue, as many different products are usually generated (often more than 10 identified products and a large amount of unidentified chemicals). To address this, innovative cell designs are being explored. For instance, the use of nanofiltration membranes was proposed to collect depolymerization products in a separate compartment and avoid degradation while facilitating separation.[144] However, the use of nanofiltration requires high pressure and is prone to membrane fouling by organic chemicals over time. It is also possible to perform lignin electrolysis at higher temperatures (100–200 °C) by dissolving lignin in pure phosphoric acid and directly soaking it on Pt anodes. In this case, the main product is CO_2, which significantly lowers the required voltage compared with water oxidation, but also strongly limits the chemical valorisation of the lignin substrate.[152] In all cases, however, anode poisoning remains an important issue for the direct electrooxidation of lignin.

Overall, the electrocatalytic oxidative or reductive valorisation of molecules involved in the value chain of lignocellulose has recently become a very active field of investigation. Several processes, particularly involving monomers, have been demonstrated to reach excellent selectivity and stability, and rapidly improving activities under ambient conditions in half-cell investigations. In the following section we detail how some of these processes have been combined into complete, fully functional electrochemical devices at the lab scale.

2.2.3 Full cell processes. While an increasingly large number of publications describe electrocatalytic measurements (voltammetry and chrono-amperometry) obtained for one specific half-reaction, reports on the performance of complete devices operating in a two-electrode configuration are scarcer. A collection of recent studies on electrochemical biomass valorisation operated in complete cells is provided in Table 1. In most cases, the oxidative or reductive valorisation processes described in the previous sections are coupled with the hydrogen evolution reaction or the oxygen evolution reaction, respectively. Indeed, coupling biomass valorisation with water dissociation has several advantages: (i) water is abundant, nontoxic, and usually used as the solvent anyway, (ii) converting the solvent essentially removes the mass transport limitation at the counterelectrode, and (iii) the evolved products (H_2 or O_2) are gaseous and can be selectively produced at the surface of electrocatalysts optimized by several decades of research work, guaranteeing a clean counterreaction. Still, some recent reports also deal with the paired oxidative and reductive valorisation of biomass-derived chemical at the anode and the cathode respectively. One immediate advantage of running these two types of process simultaneously, besides the cogeneration of valuable products, is the possibility to operate under very low cell voltages, allowing for better durability, and lower energy costs for the system. Indeed, the lowest theoretical cell potential required to drive a given electrochemical process can be approached by the difference between the standard redox potentials associated with the oxidation and reduction processes. A general ordering of these potentials on the electrochemical potential scale is provided in Fig. 4. It is clear that while, in general, little gain in operating power can be hoped for by performing biomass reduction instead of the HER (0.1–0.2 V), in contrast, replacing the OER with an oxidative valorisation process typically drastically lowers the thermodynamic requirements (more than 1 V). This opens the way for a multitude of integration strategies where value-added chemicals can be co-generated at a reduced energy cost (but at the price of increased complexity in chemical selectivity and separation). In addition to the possibility of driving these processes at low voltages compared with water splitting, it is interesting to note several instances where the oxidation and reduction products are in different phases (*e.g.* FDCA and H_2, FDCA and CO, furfuryl alcohol and O_2, methoxycyclohexanol and O_2), thus simplifying the separation and even potentially removing the need for a ionomer membrane in the system. Moreover, carboxylic acids can often be easily precipitated/crystallized out of water, while reduction products can often be

Table 1 Recent reports of full-cell electrocatalytic processes for the valorisation of lignocellulosic biomass

Reaction (oxidation and reduction)	Conditions	Ref.
HMF to FDCA and H_2 evolution 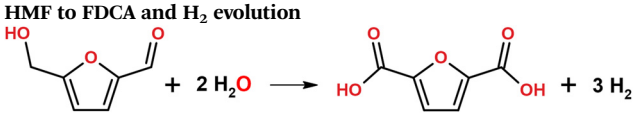	**Anode:** Pd/Ni$(OH)_2$ in 2 M NaOH + 10 mM HMF **Cathode:** 20% Pt/C in 1 M NaOH **Proton exchange membrane** (Nafion 117) FE = 97% (FDCA), E = 0.85 V, J = 12 mA cm^{-2}	100
	Anode: Co-Ni_2P in 1 M KOH + 100 mM HMF **Cathode:** Pt-coated Ti in 1 M KOH **Anion exchange membrane** (FAB-PK-130) FE = 97% (FDCA), E = 1.8 V, J = 100 mA cm^{-2}	101
HMF to FDCA and CO_2 to CO 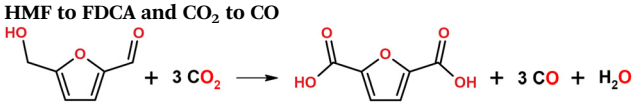	**Anode:** $NiFeO_x$/Ni foam in 1 M KOH + 10 mM HMF **Cathode:** Ni–N–C/PTFE gas diffusion electrode **Bipolar membrane** (Fumasep FBM) FE = 97% (CO) and 23% (FDCA), E = 3.1 V, J = 100 mA cm^{-2}	145
HMF to FDCA and CO_2 to HCOOH 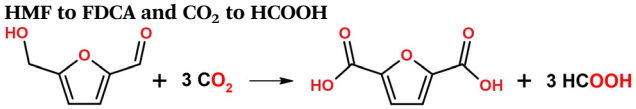	**Anode:** $NiCoO_x$/Ni foam in 1 M KOH + 0.1 M HMF **Cathode:** Cu_1Bi/C gas diffusion electrode **Anion exchange membrane** (Sustainion X37–50) FE = 90% (HCOOH) and 85% (FDCA), E = 2.35 V, J = 150 mA cm^{-2}	146
Furfural to furoic acid and H_2 evolution 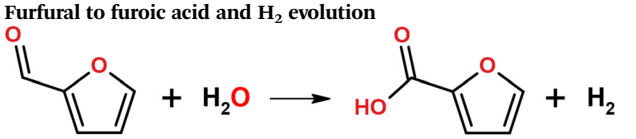	**Anode:** $NiFeO_x$/Ni foam in 1 M KOH + 0.1 M furfural **Cathode:** Pt/C electrode in 1 M KOH **Bipolar membrane** (Fumasep FBM) FE = 97% (furoic acid) and 100% (H_2), E = 2.0 V, J = 50 mA cm^{-2}	147
Glucose to glucaric acid and H_2 evolution 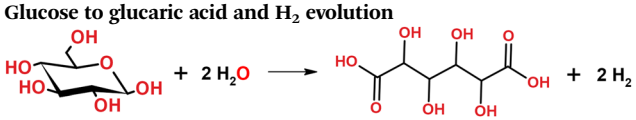	**Anode:** $NiFeO_x$/Ni foam in 1 M KOH + 0.1 M glucose **Cathode:** $NiFeN_x$/Ni foam in 1 M KOH **Anion exchange membrane** (AMI-7001) **Yield** = 54%, E = 1.4 V, J = 100 mA cm^{-2}	124
Glucose to gluconic acid and H_2 evolution 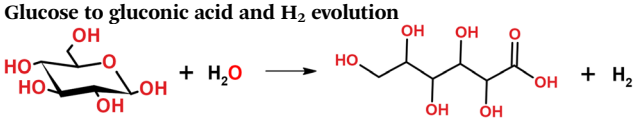	**Anode:** Pd_3Au_7/C in 0.1 M NaOH + 0.1 M glucose **Cathode:** Pt/C in 0.1 M NaOH + 0.1 M glucose **Paper separator** FE = 70% (gluconic acid) and 100% (H_2), E = 0.4 V, J = 1 mA cm^{-2}	148
O_2 evolution and furfural to furfuryl alcohol 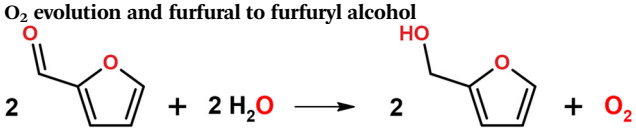	**Anode:** FeCo in 1 M K_2CO_3 **Cathode:** Cu/C in 1 M K_2CO_3 + 0.1 M furfural **Anion exchange membrane** (Sustainion X37–50) FE = 58% (furfuryl alcohol), E = 1.8 V, J = 30 mA cm^{-2}	69
O_2 evolution and guaiacol to 2-methylcyclohexanol 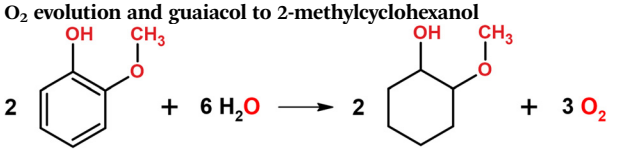	**Anode:** Ir black in 1 M NaOH **Cathode:** PtRhAu in 0.2 M $HClO_4$ + 120 mM guaiacol **Bipolar membrane** (Fumasep FBM) FE = 60% (2-methylcyclohexanol), E = 2.6 V, J = 60 mA cm^{-2}	149
HMF to FDCA and HMF to DHMTHF 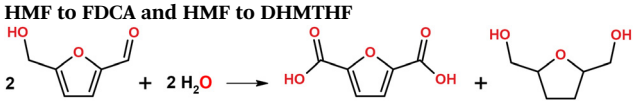	**Anode:** vanadium nitride in 1.0 M KOH + 10 mM HMF **Cathode:** Pd/vanadium nitride in 0.2 M $HClO_4$ + 10 mM HMF **Bipolar membrane** (TRJBM) E = 2.5–3.0 V, J = 100 mA cm^{-2}	150
Ethylene glycol to glycolic acid and levulinic acid to γ-valerolactone 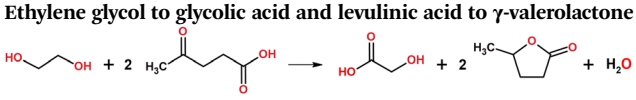	**Anode:** PtRu in 1.0 M KOH + 2 M ethylene glycol **Cathode:** PtRu/C in 0.2 M $HClO_4$ + 0.1 M levulinic acid **Proton exchange membrane** (Nafion 117) FE = 5–40%, E = 0.4–0.6 V, J = 10–30 mA cm^{-2}	151
Lignin oxidation and H_2 evolution Lignin + H_2O oxidized chemical(s) + H_2	**Anode:** PtRu in 1.0 M KOH + 10 g L^{-1} lignin **Cathode:** Pt/C in 1.0 M KOH **Anion exchange membrane** (Fumapem FAA-3–50) FE = 100% (H_2), E = 0.5–0.7 V (90 °C), J = 1–4 mA cm^{-2} (90 °C)	142

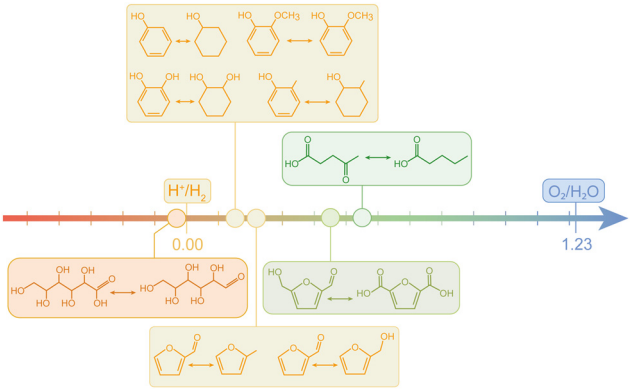

Fig. 4 Relative position of standard redox potentials associated with a selection of lignocellulose-derived chemicals on the RHE scale.

easily evaporated and condensed in a different compartment due to their high vapor pressure and low water solubility. These considerations give hope that replacing thermally-driven with electrochemical processes will afford better energy efficiency, while retaining straightforward product separation. However, it is apparent from Table 1 that, while a number of processes can be driven at reduced applied potential (*e.g.* below 1 V), current densities remain low (typically in the 10–100 mA cm^{-2} range *vs.* >1 A cm^{-2} for water electrolysers). These low current densities can be due to the low concentration of organic substrate in the electrolyte (lower than 0.1 M), which is sometimes required to achieve the desired product selectivity or to prevent the rapid poisoning or fouling of the electrode. Moreover, it is clear that directly transferring electrocatalysts from water electrolysers to biomass electrolysers can be sub-optimal. For instance, while Ni-based electrocatalysts can selectively convert HMF to FDCA in alkaline conditions, the required pre-catalytic oxidation of Ni(II) to Ni(III) occurring at *ca.* 1.4 V *vs.* RHE forces the use of very high overpotentials (typically > 1 V), leading to much higher energy losses than for the oxygen evolution reaction. This highlights a need for the development of dedicated, fine-tuned electrocatalysts for biomass valorisation, as the current generation still falls short of breaching the technology readiness level (TRL) 3–4 mark.

2.3 Photocatalytic and photoelectrocatalytic processes

Because the use of diluted substrate conditions can be required to operate biomass electrolysers with good selectivity and durability, which in turn leads to operating current densities in the 10–100 mA cm^{-2} range, it becomes interesting to directly couple solar energy conversion and electrochemical biomass valorisation in one single device. For comparison, the solar flux reaching the surface of the planet is typically converted to current densities in the order of 10–50 mA cm^{-2} in photovoltaic devices, thus providing a good match with the aforementioned requirement in biomass electrolysis. This motivates the investigation of photoelectrocatalytic and photocatalytic systems for the valorisation of lignocellulosic biomass.

2.3.1 Photocatalytic processes. Photocatalysis refers to processes where one or several light-absorbing semiconductors (usually powders of nanoparticles) are dispersed in a liquid medium containing the molecule of interest (see Fig. 5). Upon light absorption, charge carriers (electrons and holes) are generated inside the semiconductors. These charges then diffuse to the surface of the material where they can be involved (directly or indirectly) in the electrochemical conversion of the substrate of choice. Several comprehensive reviews have recently been published on the topic, and we refer the reader to them for a thorough overview of relevant materials and conditions in photocatalytic lignocellulose conversion.[153–155] In short, the photocatalytic reductions of furfural, HMF and levulinic acid have been investigated, usually in the presence of a hole scavenger (methanol, ethanol, isopropanol, triethanolamine, formic acid...). In most cases, furfural is converted to either furfuryl alcohol or hydrofuroin, HMF to 2,5-bis(hydroxymethyl)furan (BHMF) and levulinic acid to γ-valerolactone. These transformations have been conducted at the surface of a range of heterogeneous photocatalysts previously developed for hydrogen production or depollution applications (*e.g.* TiO_2, C_3N_4, $BiVO_4$, Cu_2O, $ZnIn_2S_4$...), sometimes decorated with metal co-catalysts for the reduction reaction (*e.g.* Au, Pt, Pd...).

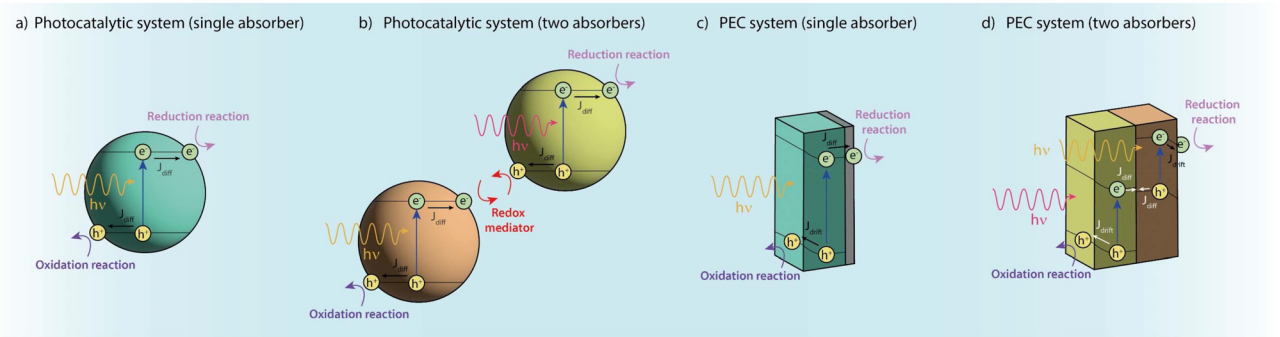

Fig. 5 Schematic representation of photocatalytic and photoelectrocatalytic (PEC) systems involving one or two light absorbers. Important differences between the two types of system include (i) a dispersed *vs.* monolithic architecture and (ii) charge transport through diffusion (J_{diff}) *vs.* drift (J_{drift}) currents.

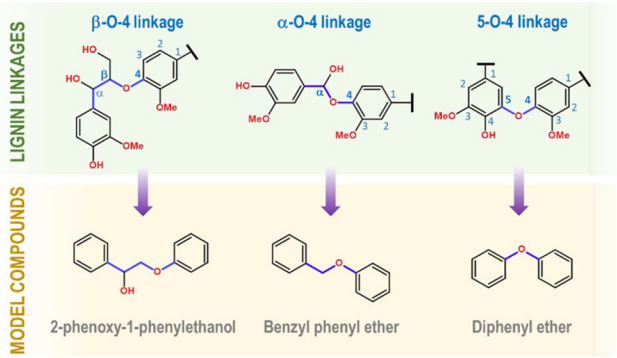

Fig. 6 Examples of model compounds used to study the redox conversion of frequent linkages encountered in lignin: β-O-4, α-O-4, 5-O-4.

Moreover, the photocatalytic valorisation of lignin has attracted a lot of interest and motivated many studies describing the photocatalytic reduction of model compounds exhibiting a β-O-4 linkage (the most frequent linkage in lignin), such as 2-phenoxy-1-phenylethanol (see Fig. 6). The photocatalytic hydrogenolysis of this compound involves the sequential oxidation of the alcohol group and reductive cleavage of the C–O bond by photogenerated holes and electrons respectively, leading to the selective formation of acetophenone at the surface of a range of (sometimes combined) photocatalysts ($ZnIn_2S_4$, TiO_2, CdS).[156–161] Furthermore, the photocatalytic reductive cleavage of α-O-4 and 5-O-4 linkages, two secondary linkages found in lignin, has been studied in the model compounds benzyl phenyl ether and diphenyl ether respectively (see Fig. 6). The photocatalytic treatment of benzyl phenyl ether by illuminated $Pd/C_3N_4/rGO/Bi_2MoO_6$ (rGO: reduced graphene oxide) leads to toluene and phenol, but can also generate cyclohexane when the loading of Pd exceeds 3%.[162] Similarly, diphenyl ether can be reduced to cyclohexane and cyclohexanol by photocatalysts loaded with Pt or Pd in excess of 3%.[162,163] On the other hand, the photocatalytic oxidation (or reforming) of lignocellulose and/or its components has gathered interest as it combines hydrogen production with biomass valorisation. For instance, a CdS/CdOx photocatalyst has been shown to efficiently perform the reforming of lignocellulose under illumination in alkaline conditions,[164] producing up to 5–6 mmol(H_2) g_{cat}^{-1} h^{-1}. While the oxidation products were not identified in full, the production of formate and carbonate was confirmed. When it comes to fractionated lignocellulose, the photocatalytic reforming of cellulose has been studied on several photocatalysts: Pt/TiO_2,[165,166] $RuO_2/Pt/TiO_2$,[167] and Ni_xS_y/TiO_2,[168] In these reports, CO_2 is usually assumed to be the main oxidation product, but glucose and HMF were also detected. Interestingly, using TiO_2 decorated with acidic zeolite and Au nanoparticles inside an ionic liquid at 140 °C yields a mixture of glucose and HMF (59% maximum total conversion yield after 16 h for 50 mg of cellulose and 50 mg of photocatalyst) under visible light irradiation.[169] This demonstrated that using multifunctional photocatalysts can be a successful strategy to control the selectivity of cellulose oxidation under illumination (producing high-value products rather than CO_2). Finally, photocatalytic conversion of platform compounds such as glucose, furfural or HMF has also been investigated on inorganic and organic photocatalysts.[66,170–176]

Overall, photocatalytic processes have shown promising selectivity and photon yields for the reductive and oxidative valorisation of lignocellulosic platform and model compounds. However, most studies are limited to small (<10 mL) laboratory-scale batch demonstrators in dilute conditions (a few mM of substrate). Moreover, reductive photocatalytic approaches often require the use of sacrificial scavengers to harvest unused photogenerated holes, with the notable exception of the aforementioned conversion of 2-phenoxy-1-phenylethanol. It is therefore difficult to imagine the deployment of large-scale photocatalytic biorefineries in the near future. Still, the selectivity and technical simplicity associated with photocatalytic processes make them interesting for the production of small-scale high-value specialty chemicals from biomass-derived platform compounds. An alternative to photocatalysis to power chemical transformations with photons at higher rates is the use of photoelectrochemical systems, presented in the following section.

2.3.2 Photoelectrocatalytic processes. A photoelectrochemical (PEC) system is an electrochemical cell where one or both electrodes is a photoabsorber (producing a so-called photoelectrode), thus allowing for direct solar-to-chemical transformations. Upon immersion of a photoelectrode inside an electrolyte, an equilibration of the Fermi levels, or electrochemical potential, of the semiconductor and the electrolyte occurs, leading to the establishment of a permanent electric field at the semiconductor–liquid junction (SCLJ). This electric field induces a band bending inside the semiconductor, the direction depending on its polarity. This band bending, absent from photocatalytic systems, allows the formation of drift currents (typically larger than diffusion currents) for photogenerated charges, and improved charge separation (see Fig. 5). An additional advantage of PEC compared with photocatalysis is the possibility to apply a potential bias to the photoelectrode, thus favouring charge separation as well as tuning the adsorbate–electrode interactions for a better selectivity.[175] To perform a PEC oxidation reaction, an n-type absorber is required to form a photoanode. In this case the band system is bent upward at the SCLJ, inducing hole transfer to the electrolyte. Conversely, photocathodes for reduction reactions are produced from p-type absorbers, generating a downward band bending at the SCLJ, and thus inducing electron transfer to the electrolyte. Finally, just as in photocatalysis, photoelectrodes can be coated with active and selective electrocatalysts to improve efficiency. Overall, with proper band alignment, connecting a photoelectrode and a dark counter-electrode or two photoelectrodes in series affords a PEC device capable of operating the direct conversion of solar energy into chemical energy. As for the other approaches, PEC can be used to oxidize or reduce biomass-derived molecules or raw biomass

components. Research on the lignocellulosic biomass solar valorisation has been heavily inspired by previous research on PEC water splitting, and stable photoanodes and photocathodes developed in this context have been transferred to PEC biomass valorization. Photoanodes are thus generally composed of n-type oxides while photocathodes are composed of p-type semiconductors spanning over a wide array of materials families, including oxides (*e.g.*, Cu_2O), chalcogenides (*e.g.*, Sb_2Se_3), nitrides (GaN), phosphides ($GaInP_2$) and covalent semiconductors (*e.g.*, Si). Here, we propose a brief overview of the state-of-the-art, but we would also like to direct the reader towards several recent reviews for more technical details on this topic.[177–180] A summary of the most relevant reports for PEC lignocellulose valorization, discussed hereafter, is provided in Table 2. The direct oxidation of cellulose has been demonstrated with TiO_2 and $SrTiO_3$ photoanodes in photofuel cells coupling biomass oxidation and oxygen reduction reaction.[181,182] In these reports, cellulose was fully converted to CO_2 but intermediate carboxylic acids (*e.g.*, formic, malonic, oxalic, and gluconic) were detected during the reaction.[181] In particular, the production of CO_2 on TiO_2 soared after one hour of illumination at 1 V *vs.* RHE in 2 M NaOH. Before 1 h, malonic, glyceric, and formic acid were the main products of the reaction, highlighting that milder oxidations conditions are required to produce valuable molecules from cellulose.[182] Surface modification of TiO_2 with Bi_2O_3 and $CuBi_2O_4$ was further employed to steer the selectivity of cellulose oxidation towards formate, while inhibiting the oxygen evolution reaction, reaching an FE of 83.9% at 0.5 V *vs.* RHE after two hours of illumination in 0.1 M NaOH.[183] We note that there are very few reports available on PEC cellulose oxidation. One reason for this is the easy hydrolysis of cellulose into glucose and its subsequent dehydration to HMF, enabling the development of easier and more controlled PEC processes on these platform compounds. The PEC oxidation of glucose was initially investigated for electricity production in photofuel cells, yielding mostly CO_2 and CO.[177,194] In a seminal study, WO_3 was used as photoanode for the solar-driven oxidation of glucose into added-value products including gluconic and glucuronic acids, erythrose and arabinose.[184] The use of Na_2SO_4 or CH_3SO_3Na electrolyte allowed the production of glucuronic acid at pH 4, while this product was absent when NaCl was used. The authors hypothesized that $SO_4^{\bullet-}$ and $CH_3SO_3^{\bullet}$ radicals generated upon irradiation of the WO_3 photoanode were responsible for this selectivity. In a later study, a $CuWO_4$ photoanode, showing improved stability compared with WO_3, was reported for the production of formate from glucose (FE = 76%) at pH 10.2.[195] Elsewhere, UV-irradiated anodized nanotubular Ti/TiO_2 was reported to convert 78% of glucose into a mixture of gluconic acid, arabitol, and arabinose after 3 h of reaction at 1.5 V *vs.* Ag/AgCl in 0.1 M Na_2SO_4 (pH 6.6).[196] In another study, Pt-decorated TiO_{2-x} nanotubes were found to be highly selective towards the production of glucaric acid with a yield of 84.3% at 0.6 V *vs.* RHE in 1 M KOH. This excellent yield was attributed to a favorable interaction between surface defects and Pt single atoms.[197] Finally, more complex architectures such as a Fe_2O_3/CuO heterojunction were proposed for the selective production of formate, achieving a remarkable FE of 94.1% and a turnover frequency of 240.2 h^{-1} at 1.5 V *vs.* RHE in 0.1 M NaOH.[198] The direct PEC oxidation of HMF was investigated on various photoelectrodes: WO_3 (pH 4), $BiVO_4$ (pH 9.2), and Fe_2O_3 (pH 14). While the *J–V* curves of illuminated Fe_2O_3 and $BiVO_4$ were mainly unchanged in the presence of HMF, improvements in both photovoltage and photocurrent densities were observed for WO_3. Thus, at 3 suns, with an applied potential of 0.68 V *vs.* RHE and 64 hours of continuous operation, modest yields for FFCA (4%) and FDCA (0.5%) were measured at a WO_3 photoanode.[186] Alternatively, the simultaneous PEC-assisted oxidation of HMF and HER has been investigated using bare and phosphate-functionalized phosphorene-sensitized $BiFeO_3$, resulting in the production of FDCA with a conversion yield of 100%.[189] In this case, *in situ* Raman spectroscopy revealed that the oxidation mechanism of HMF to FDCA involved catalyst-bound reactive oxygen species such as M-OH, M=O, and M-OOH, participating in an indirect mechanism (see section 2.2). Finally, a tubular Ti/TiO_2/Pt photoanode was irradiated under a 365 nm UV light to convert 0.5 mM of HMF at various biases and pH.[199] However, for reaction times above 120 min, conversions of only about 10–12% were achieved, with a product selectivity below 40%. Moreover, the use of TEMPO as a redox mediator for the indirect PEC oxidation of HMF has been extensively studied. It was first demonstrated with pristine $BiVO_4$ (pH 9.2) where HMF was converted to FDCA (yield >98%) at 1.04 V *vs.* RHE under 1 sun.[113] Later, improved TEMPO-mediated HMF oxidation was demonstrated over $BiVO_4$/NiFe-LDH[200] and $BiVO_4$/CoPi[201] at lower applied potentials (≈0.6–0.7 V *vs.* RHE). TEMPO was also used to mediate and promote HMF oxidation on F:Fe_2O_3/FeOOH[202] and Ti:Fe_2O_3/CoPi[203] photoanodes. With the former, the conversion of 10 mM HMF was only about 11.7% at pH 12.5 after 20 h under illumination, while the addition of TEMPO drastically raised the conversion to 99.2% after only 5.5 h. Interestingly, without TEMPO, HMFCA (83.9%) was the main product, whereas with 2 g L^{-1} TEMPO, FDCA became the dominant product (90.7%). For Ti:Fe_2O_3/CoPi, with 6.5 mM TEMPO, after 60 C of total charge had passed, FFCA (≈55%) and FDCA (≈42%) were the main products. Finally, TEMPO was used to mediate the conversion of HMF to FDCA with a high faradaic efficiency of 80% after 2 h of reaction over perylene diimide-sensitized Sb:SnO_2 photoanodes.[204]

While PEC conversion of cellulose and its derivatives can proceed relatively easily, the direct PEC oxidation of lignin is much more challenging due to the its low solubility in aqueous media and its strong absorption of UV and visible light.[178] Still, several interesting reports can be found in the literature. In an early study, a Ti/$Ru_{0.1}Sn_{0.6}Ti_{0.3}O_2$ photoanode was operated under UV light at very high potential (2 or 6 V *vs.* SCE at pH 11). After 6 h of PEC treatment of a 2 g L^{-1} lignin solution, total organic carbon and total phenol abatements of 51% and 83%, were respectively measured, but no information on the nature of the oxidation products was provided.[205] More

Table 2 Selection of state-of-the-art reports on photoelectrochemical lignocellulosic biomass valorization

Substrate	Cathode	Anode	Catholyte (pH), anolyte (pH)	Illumination	Bias (V *vs.* RHE)	J (mA cm^{-2})	Products (yield)	Product FE (%)	Ref.
α-Cellulose 100 g L^{-1}	Pt foil	FTO/TiO_2	0.1 M NaOH (13)	Solar simulator (100 mW cm^{-2})	0.5	0.42	Rate: 1 μmol cm^{-3} h^{-1}	FA (25%)	183
		FTO/TiO_2/Bi_2O_3				0.39	3 μmol cm^{-3} h^{-1}	FA (84%)	
Glucose 100 mM	Pt grid	FTO/WO_3	0.1 M CH_3SO_3Na (2) 0.1 M $NaHSO_4$ (2) 0.1 M NaCl (2) 0.1 M $NaClO_4$ (2)	150 W solar simulator (100 mW cm^{-2})	1.23	n/a	Gluconic acid, glucaric acid, erythrose, arabinose	n/a	184
Glucose 500 mM	CsFAMA/Pt	$Cu_{30}Pd_{70}$	1 M KOH (pH 14)	Solar simulator (100 mW cm^{-2})	n/a	8.5	Gluconic acid	Gluconic acid (65%)	185
HMF 5 mM	Pt wire	FTO/WO_3	0.1 M NaPi (4)	3 suns (300 mW cm^{-2})	0.68	0.1–0.3	FFCA (4%), FDCA (0.5%)	n/a	186
HMF 5 mM	Pt film	FTO/$BiVO_4$	0.5 M borate buffer (9.2) + 7.5 mM TEMPO	Solar simulator (100 mW cm^{-2})	1.04	>0.5	FDCA (98.85%), FFCA (0.36%), DFF (0.01%), HMFCA (0.025%)	FDCA (93%)	113
HMF 20 mM	Cu/Ag	FTO/$BiVO_4$/NiOOH	0.5 M borate buffer (9.2) 0.5 M borate buffer + 1 M Na_2SO_3 (9.2)	Solar simulator (300 mW cm^{-2})	0.92	1	BHMF (96–99% selectivity)	BHMF (89–96%)	187
HMF 10 mM	p-Si/$Ni_{0.95}Pt_{0.05}Si$	n-Si/$Ni_{0.95}Pt_{0.05}Si$	0.5 M H_2SO_4 1 M KOH (14)	500 W Xe lamp (100 mW cm^{-2})	n/a	5	HMFCA (45.0%), FDCA (27.3%)	n/a	188
HMF 5 mM	FLP-P-$BiFeO_3$	FLP-P-$BiFeO_3$	0.5 M Na_2SO_4	200 W simulator (50 mW cm^{-2})	1.39	20	FDCA (100%)	n/a	189
PPE 1 mM	Graphite rod	C/CoO/P: $MnCO_3$	1 M KOH, 30 wt% MeOH	Solar simulator (100 mW cm^{-2})	1.7	20	Benzoic acid (49%), phenol (49%)	>97%	190
TMBA 1 mM	C/CoO/P: $MnCO_3$	Graphite rod	1 M KOH, 30 wt% MeOH	Solar simulator (100 mW cm^{-2})	−0.5	−20	DMPE (48%), MMPE (46%)	>97%	190
Kraft lignin 0.25–1.5 g L^{-1}	Si/mesoITO	FTO/Fe_2O_3	Acetonitrile/water (v/v 1 : 1) TEOA-buffer, 1 mM NADH, 25 mM $MgSO_4$, 6 μM TsOYE, 9 mM MCO	Solar simulator (100 mW cm^{-2})	n/a	1.5	Methyl 2-hydroxybenzoate, (4-isopropylphenyl) methanol, diethyl phthalate, terephthalic acid, (tetramethoxy-6-methylphenyl)ethanone	n/a	191
Lignosulfonate 5 g L^{-1}	Carbon cloth	FTO/$BiVO_4$/PV perovskite	0.1 M phosphate buffer (6.5) + 2 mM NAD^+ + 0.5 mM $[Cp^*Rh(bpy)H_2O]^{2+}$ 0.01 M $KHCO_3$ (pH 8.2)	450 W Xe lamp (100 mW cm^{-2})	n/a	n/a	Butanedioic acid, glycolic acid, benzoic acid, *N*-methoxymethyl-*N*-methylformamide, 1,1,3,3-tetrachloroacetone, and *N*-methyl-*N*(2-methylpropyl)formamide	n/a	192
Lignocellulosic biomass[a] 37.5 g L^{-1}	ITO/CsFAMA/FM/Pt-Ti	MWCNT	0.5 M H_2SO_4 0.5 M H_2SO_4 + 0.25 M PMA	300 W Xe lamp (100 mW cm^{-2})	n/a	−19.8	Vanillin, acetovanillone	n/a	193

FTO = F-doped SnO_2, HMF = 5-hydroxymethylfurfural, FFCA = 5-formyl-2-furoic acid, FDCA = furan dicarboxylic acid, DFF = diformylfuran, HMFCA = 5-hydroxymethl-2-furoic acid, BHMF = 2,5-bis(hydroxymethyl)furan, FLP = phosphate-functionalized phosphorene, PPE = 2-phenoxy-1-phenylethanol, TMBA = 3,4,5-trimethoxybenzylalcohol, DMPE = 3,4-dimethoxyphenylethanol, MMPE = 2-methoxy-4-methylphenol, CsFAMA = cesium formamidinium methylammonium perovskite, FM = Field's metal, PMA = phosphomolybdic acid, TEOA = triethanolamine, Cp* = C_5Me_5, bpy = 2,2′-bipyridine, NADH = nicotinamide cofactor, TsOYE = yellow enzyme homologue from *Thermus scotoductus*, MCO = 2-methyl-2-cyclohexen-1-one, MHB = methyl 2-hydroxybenzoate, IPM = 4-(isopropylphenyl)methanol, TMME = 1-(2,3,4,5-tetramethoxy-6-methylphenyl)ethenone. [a] Reacted with 0.25 M PMA at 60 °C for 12 h.

recently, a biased Ti/TiO_2/Ta_2O_5-IrO_2 photoanode was used to oxidize lignin in 0.5 M NaOH at 0.6 V *vs.* Ag/AgCl under UV light.[206] After 2 h, 66% and 92% of lignin was degraded in dark and light conditions, respectively. The production of vanillin and vanillic acid was confirmed by HPLC.[206] Likewise, Kraft lignin was oxidized onto TiO_2 nanoparticles deposited on FTO glass after applying a potential of 2.3 V under UV irradiation.[207] The PEC oxidation of Kraft lignin was also investigated on an α-Fe_2O_3 photoanode grown on a transparent FTO substrate in a mixture of acetonitrile and deionized water (v/v = 1 : 1).[191] Terephthalic acid, methyl 2-hydroxybenzoate, and diethyl phthalate were identified as oxidation products but no quantitative study was performed. Interestingly, the illuminated back of the photoanode was in contact with the glass container so that the light passed through the absorbing layer of the photoelectrode before being absorbed by the lignin, illustrating the advantage of using transparent conductive substrates in PEC reactor design for lignin valorisation. The PEC oxidation of Kraft lignin was finally combined with the PEC enzymatic asymmetric hydrogenation of C=C bonds in 2-methyl-2-cyclohexen-1-one inside a stand-alone solar-powered device biased with a Si photovoltaic panel.[191] In another study, a tandem $BiVO_4$/PV perovskite structure allowed the unbiased oxidation of lignosulfonate and alkali lignin under visible light. In parallel, carbon cloth was connected to the system for the reduction of CO_2 using redox enzymes and cofactors. Lignin was broken down to small carboxylated organic molecules such as butanedioic acid and glycolic acid.[192]

Similar to photocatalytic systems, the PEC oxidation of model lignin molecules exhibiting a β-O-4 linkage (see Fig. 6) has been studied in several systems. $BiVO_4$ and $BiVO_4$/V_2O_5 anodes were efficient at oxidizing 0.25 mmol of model lignin derivatives at 2.0 V *vs.* Ag/AgCl in 0.1 M $LiClO_4$ with 25 mL MeCN.[208] Aryl aldehyde and phenol derivatives were formed with a conversion up to 64% over 20 h. Elsewhere, F:Fe_2O_3/Co:NiO_xH_y was found to provoke highly selective C_α–C_β cleavage of lignin dimers at 1.48 V *vs.* RHE in 1 M NaOH. Especially, the authors stressed the critical role of Ni(IV) active sites, preferentially formed at higher working voltages, to obtain aromatic carboxylic acids at high yields (85.0–99.8%).[209] In other studies, lignin dimers were oxidized using dye-sensitized TiO_2 photoanodes and hydrogen atom transfer mediators such as 4-acetamido-2,2,6,6-tetramethyl-1-peperidine-*N*-oxyl (ACT), phthalimide-*N*-oxyl (PINO), and 9-azabicyclo[3,3,1]nonan-3-one-9-oxyl (KABNO).[210–212] A PEC method was also recently developed to depolymerize lignin and selectively hydrogenate and deoxygenate the aromatic ring terminals for the preparation of aviation fuel precursors.[190] CoO/$MnCO_3$ was used as a photoelectrode to cleave the β-O-4 linkage of 2-phenoxy-1-phenylethan-1-ol (1 mM) at 1.5 V *vs.* RHE under illumination in 1 M KOH. Furthermore, hydrogenation and deoxygenation processes were achieved using 1 mM of 3,4,5-trimethoxybenzylalcohol in the same conditions but at a cathodic potential of −0.5 V *vs.* RHE. Interestingly, the β-O-4 linkage of 2-phenoxy-1-phenylethan-1-ol could be cleaved in cathodic and anodic conditions. In cathodic conditions, only 1-phenylethanol and phenol were produced but without further hydrogenation. In contrast, 3,4,5-trimethoxybenzylalcohol was fully converted to 3,4-dimethoxyphenylethanol and 2-methoxy-4-methylphenol after 2 h of reaction. All these studies show that it is possible to convert lignin or (more often) lignin-derived oligomers, monomers and model compounds in PEC processes, although product identification remains a challenge.

The reports described so far for PEC lignocellulose valorisation all require the application of a substantial potential bias to drive the electrochemical conversion of lignocellulosic compounds. In contrast with these "assisted" configurations involving polarized photoelectrodes, we devote the last part of this section to reports of stand-alone, unbiased PEC devices capable of using sunlight as an exclusive source of energy to drive lignocellulosic biomass valorisation. Such a PEC device has been proposed for the simultaneous cellulose oxidation at the photoanode (Ti:α-Fe_2O_3/NiOOH) and CO_2 reduction at the photocathode (Si/Bi/GaN).[213] In this study, the authors report the production of formate at both sides of the cell, with an overall yield of 23.3 μmol cm^{-2} h^{-1}. They further demonstrated the PEC production of formate from raw biomass sources such as sawdust, straw, and bamboo. However, in these cases, an acidic pre-treatment step was necessary to remove the insoluble lignin and depolymerize the hemicellulose components to mono- and disaccharides. The FE for formate was consistently higher than 90% for all biomass sources when the photoanodic side was studied alone. Elsewhere, an unbiased device allowed the oxidation of glucose over a Ni/$Cu_{30}Pd_{70}$ anode while H_2 was produced at a hybrid halide perovskite photocathode with a photocurrent of 8.5 mA cm^{-2} under one sun. After 10 h of operation, glucose was converted to gluconic acid with a selectivity of 65%.[185] Regarding HMF valorisation, a PEC device involving an n-Si/$Ni_{0.95}Pt_{0.05}$Si photoanode for HMF oxidation and p-Si/$Ni_{0.95}Pt_{0.05}$Si photocathode for HER was recently reported.[188] The system was able to generate photocurrent densities as high as 5 mA cm^{-2} in the presence of 10 mM HMF in 1 M KOH as the anolyte with a high HMF conversion (97.2%) and FDCA yield (80.3%). Another PEC cell involving a Cu/Cu_2O photoanode and p-Si/CdS/Pt photocathode was reported for the oxidation of 30–100 mM HMF in 1 M KOH. Remarkable photocurrent densities of 15 mA cm^{-1} were achieved with a good FE for HMFCA (84%).[214] Finally, regarding the valorisation of lignin-containing biomass, an indirect PEC device was demonstrated to produce vanillin and acetovanillone from lignocellulose. In a pre-treatment step, the lignocellulosic biomass was incubated with phosphomolybdic acid (PMA) at 60 °C for 12 h. This step oxidized mostly the lignin within the biomass to products of interest while reducing the PMA. The unbiased PEC cell with ITO/CsFAMA/Pt–Ti as a photocathode and multi-walled carbon nanotubes as the anode was then used to regenerate PMA, while producing H_2 at a high photocurrent density of 19.8 mA cm^{-2}.[193]

Overall, while photocatalytic and photoelectrocatalytic systems hold promises for the direct solar valorisation of lignocellulosic biomass, their implementation remains limited to the lab scale, due to stringent limitations in stability and scal-

ability, despite the recent demonstration of several stand-alone PEC devices for biomass valorisation. An important aspect that emerges from this literature involves a direct technology transfer from decades of work on water splitting. However, one should keep in mind that (i) there is no reason that the best-performing photoanodes for water splitting should necessary be the most efficient for biomass valorisation (in particular due to the strong interaction of organic substrates with the photoelectrode surface, leading to potential challenges in selectivity or poisoning) and (ii) many materials with improper band alignments were not investigated in the context of water splitting but could outperform the currently tested semiconductors for biomass valorisation. As such, many opportunities remain to be explored in the field of PEC biomass valorisation, especially through the development of materials and device architecture designed around the specific advantages and challenges of biomass upgrading compared with water splitting. This includes for instance operation at low voltage, tolerance to poisoning by carbon-based intermediates, selective cleavage of specific functional groups, the possibility of tandem electrocatalytic schemes for cascade or concerted chemical transformations, preservation of selectivity in the presence of complex mixtures, exploitation of mixed-solvent electrolytes, *etc*. As such, while there is interest in developing these technologies for future generations of highly integrated solar biorefineries, it is currently difficult to assess their viability on an industrial scale. Indeed, photocatalytic and PEC systems for biomass valorisation are currently mainly studied at TRL 3 or below. This means that while current research mainly focuses on benchmarking activity and selectivity over the course of a few hours to several days, many important challenges remain to be addressed in the future, such as catalyst long-term stability and replacement/regeneration cost, or system integration and optimization with considerations of low-grade heat recovery and use, electrolyte recycling, product separation, *etc*. Still, this also represents a great opportunity to conceive and develop innovative photoabsorbers and electrocatalysts specifically tailored towards lignocellulose valorisation and beginning charting a novel area in PEC research through material development and device engineering.

At the moment, biomass electrolysers powered by renewable (*e.g.* solar or wind) electricity appear as the most attractive technology. Then, to try and determine whether including electrocatalytic processes in biorefineries holds promise in the current and future energy landscape, we present a comparative study between defossilized *electrified catalytic hydrogenation* and *electrocatalytic hydrogenation* in the following section. For this we propose to base our analysis on the example of furfural valorisation, a process currently under study in our research laboratory.

3. A case study on furfural valorization

In an attempt to evaluate the industrial potential of direct use of solar energy for biomass valorisation, we consider the electrochemical hydrogenation performed by a biomass electrolysis unit coupled to photovoltaic (PV) electricity. As extensive research and development have been performed in the past decades to develop electrolysers into more mature systems, technological spillovers can benefit biomass electrolysers for their industrial development, bringing them closer to industrial relevance. In the meantime, solar PV has benefited from scaling economics[215] allowing for the levelized cost of electricity (LCOE) of current new projects to reach prices below 45 $ per MWh.[216]

As such, combining both technologies potentially allows for high solar to fuel efficiency at a lower price than other solar-based pathways. As developed in the previous section, electrochemical hydrogenation (ECH) of furfural has received attention lately as an alternative to thermochemical hydrogenation: the direct use of renewable electricity is expected to lower the carbon footprint of the conversion step at market parity costs. To verify these assumptions, we present an energy efficiency analysis, followed by a basic economic assessment of the electrochemical hydrogenation of furfural towards furfuryl alcohol (FOH) and 2-methylfuran (2MF). This analysis aims to evaluate furfural conversion step costs within realistic assumptions (*e.g.* electricity price, stack cost). For this initial calculation, separation costs, labor and taxes were not considered. Separation energy requirements, especially when the product is in aqueous phase like in ECH, can become important, thus increasing the separation costs. However, in the absence of a reference process, the estimation of such costs was not performed. Future studies could elucidate this point to provide a better estimate. Thermocatalytic furfural hydrogenation into FOH or 2MF is industrially performed on copper chromite catalysts with furfural either in the liquid or gas phase and under pressure of H_2 gas. Temperature and pressure conditions will vary accordingly to the desired product and the reactant phase.

Table 3 Typical operating conditions for furfural thermochemical hydrogenation[217–219]

	Furfuryl alcohol		2-Methylfuran	
	Liquid phase	Gas phase	Liquid phase	Gas phase
T (°C)	120	122–152	200	200–250
Solvent	Water, isopropanol, ethanol	—	Isopropanol, ethanol	—
Furfural: solvent ratio	1 : 10	—	1 : 10	—
Catalyst	Pd, copper chromite	Copper chromite	Pd, copper chromite	Copper chromite
$kg_{H_2}\ t^{-1}$	21		49	

The typical operating conditions used in our analysis are summarised in Table 3. Importantly, in the context of this analysis, we consider that the H_2 required for the hydrogenation of furfural is produced through electrochemical water splitting since it remains to date the only scalable, low-carbon and high-TRL way of producing decarbonized hydrogen.[220] Therefore, the energy intensity of the overall processes can be evaluated considering:

(i) *The energy required to produce electrolytic hydrogen*. We use an estimated value of 59 kWh $kg_{H_2}^{-1}$ or 212.4 GJ $t_{H_2}^{-1}$,[221,222] and we further estimate that the synthesis of 1 ton of 2MF requires 49 kg_{H_2} while 21 kg_{H_2} is necessary for 1 ton of FOH.

(ii) *The thermal energy contribution*. We calculate the necessary enthalpy ΔH to raise reactants and solvents (when present) from room temperature to reaction temperature (ΔT) using the heat capacity of furfural and the solvent ($C_{p,furfural}$ and $C_{p,solvent}$ respectively):

$$\Delta H = (C_{p,furfural} + C_{p,solvent})\Delta T \quad (1)$$

For gas phase reactions, the contribution of the enthalpy of vaporization of furfural is considered:[223]

$$\Delta H_{vap,furfural} = 50.7 \text{ kJ mol}^{-1}$$

(iii) *Thermal losses and waste heat recovery* are not considered in our analysis, as a first approximation.

We find that, compared with vapor phase hydrogenation, liquid phase reactions require more energy (5.1 *vs.* 5.8 GJ t_{FOH}^{-1} & 11.7 *vs.* 14.3 GJ t_{2MF}^{-1}) for both products because of the energy required to heat the solvent, taken as ethanol (resp. 0.7 and 2.6 GJ t^{-1}) (see Fig. 7a). Indeed, in gas phase hydrogenation, only furfural must be heated which reduces the energy intake by ~10–20% compared with liquid phase. We note that G. Fraga *et al.* found a heating value of 3 GJ t_{FOH}^{-1} (including separation) in their liquid-phase process analysis, which supports the validity of our estimate.[224] Furthermore, we note that this heating penalty in ECH and liquid phase synthesis is likely to be increased during the separation step as energy is required to separate product and solvent. However, regarding 2MF generation in water (typical ECH conditions), product separation is facilitated due to the high volatility of 2MF and its low solubility in water.[218,225] Next, to compare the energy intensity of furfural hydrogenation under electrocatalytic and the aforementioned thermocatalytic conditions, the energy intensity of the electrocatalytic process was estimated using the following equation, derived from D. Jin *et al.* and Bard:[226,227]

$$E_{ECH}\,[\text{GJ t}^{-1}] = \frac{n \cdot F\,[\text{C mol}^{-1}] \cdot U\,[\text{V}]}{M\,[\text{g mol}^{-1}] \times 1000 \times \frac{\text{FE}\,[\%]}{100}} \quad (2)$$

with n the number of electrons exchanged during the reaction, F the Faraday constant, U the cell voltage, M the molar mass of the product, and FE the faradaic efficiency towards the product. Due to the thermodynamics (equilibrium potentials) and kinetics (overpotentials, ohmic losses) of the process, a cell voltage threshold to perform the ECH of furfural will exist. By considering the OER as the counter-reaction of furfural ECH to FOH or 2MF, we built a diagram displaying the thermodynamics and kinetics contribution as a function of cell voltage and current density for these two processes (see Fig. 7b). More specifically, anodic and cathodic overpotentials were estimated by considering only the forward (resp. back-

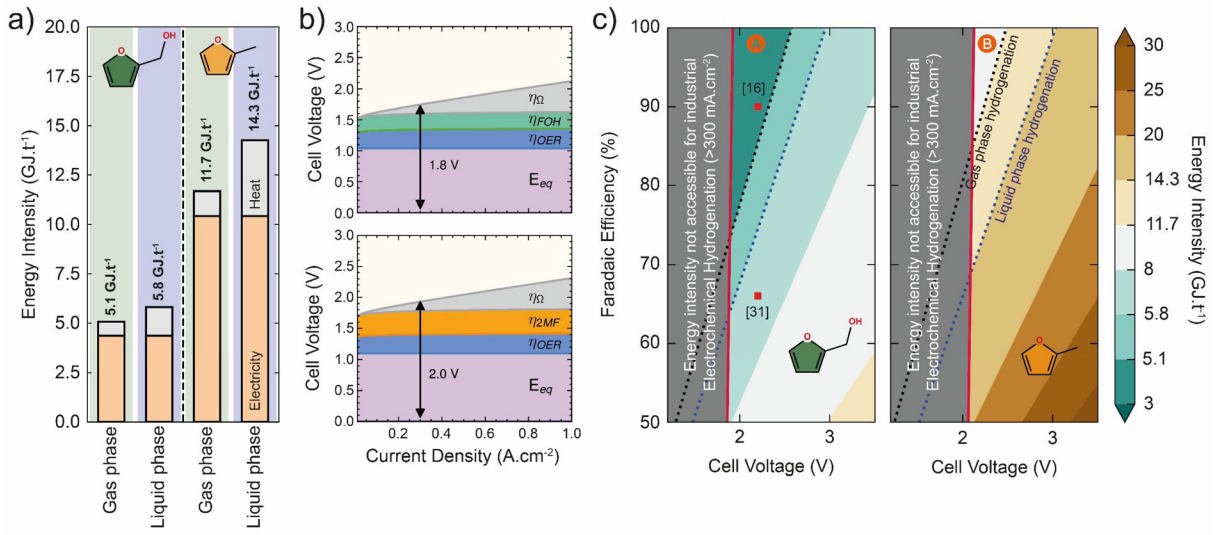

Fig. 7 (a) Comparison of the energy requirements for liquid and gas phase hydrogenation of furfural to furfuryl alcohol (left) and 2-methylfuran (right). (b) Stacked kinetic plots of furfural electrochemical hydrogenation to furfuryl alcohol and 2-methylfuran (contributions from bottom to top: equilibrium potentials, OER overpotential, furfural ECH overpotential, ohmic drop losses). (c) Contour plot of furfural electrochemical hydrogenation energy intensity as a function of product faradaic efficiency and cell voltage as calculated from eqn (2). Red lines indicate the minimum energy intensity at industrial current densities as estimated from the voltage of the stacked kinetic plots at 300 mA cm^{-2} and a fixed energy consumption of 0.24 and 0.59 GJ t^{-1} for FOH and 2MF respectively.

ward) reaction rates in the Butler–Volmer equation, under the form of Tafel equations:[228]

$$\eta_{FOH} = \frac{R\,[\mathrm{J\,mol^{-1}\,K^{-1}}]\cdot T\,[\mathrm{K}]}{n_{FOH}\cdot F\,[\mathrm{C\,mol^{-1}}]\cdot \alpha}\ln\frac{j\,[\mathrm{A\,cm^{-2}}]}{j_{0,FOH}\,[\mathrm{A\,cm^{-2}}]} \quad (3)$$

$$\eta_{2MF} = \frac{R\,[\mathrm{J\,mol^{-1}\,K^{-1}}]\cdot T\,[\mathrm{K}]}{n_{2MF}\cdot F\,[\mathrm{C\,mol^{-1}}]\cdot \alpha}\ln\frac{j\,[\mathrm{A\,cm^{-2}}]}{j_{0,2MF}\,[\mathrm{A\,cm^{-2}}]} \quad (4)$$

$$\eta_{OER} = \frac{R\,[\mathrm{J\,mol^{-1}\,K^{-1}}]\cdot T\,[K]}{n_{OER}\cdot F\,[\mathrm{C\,mol^{-1}}]\cdot \alpha}\ln\frac{j\,[\mathrm{A\,cm^{-2}}]}{j_{0,OER}\,[\mathrm{A\,cm^{-2}}]} \quad (5)$$

where R is the gas constant, T the temperature, n_i is the number of exchanged electrons for the synthesis of product i, F is the Faraday constant, α is the transfer coefficient, and j_0 is the exchange current density for the considered reaction. Values were obtained from experimental results described in the literature and are reported in Table S1.† On the basis of the obtained kinetic plot, a cell potential operating at industrial current densities (*i.e.* above 300 mA cm^{-2}, see below) is estimated at a minimum of 1.8 and 2.0 V for FOH and 2MF synthesis, respectively. Consumption of utilities for the balance of plant (power equipment, pumps, water treatment, gas separators...) of the electrochemical process is also accounted and estimated at 5% of the energy required for vapour-phase hydrogenation (0.24 and 0.59 GJ t^{-1} of FOH and 2MF respectively, see Fig. 7a).

Fig. 7c represents faradaic efficiency *vs.* cell voltage plots for FOH and 2MF production by ECH. These graphs inform on the energy consumed to produce one ton of each product through electrocatalysis based on eqn (1). For a given production rate (*i.e.* current density), when the cell potential is reduced and the faradaic efficiency increases, less energy is required to perform the conversion. Moreover, based on the aforementioned minimum operating potential and utilities consumption, we estimate that the only conversion energies accessible to industrial furfural ECH are localized at cell potentials higher than the ones indicated by the red lines. From these calculations, we conclude that a furfural electrolyser running at a cell voltage below 2.44 V (2.51 V for 2MF) and a FE higher than 80% (85% for 2MF) would operate with a better energy efficiency than vapor-phase hydrogenation from electrolytic H_2. The conditions in which furfural ECH is more energy-efficient than vapor-phase hydrogenation are indicated as *zone A* for FOH and *zone B* for 2MF on Fig. 7c. On this figure, we also display the literature results of continuous electrocatalytic hydrogenation of furfural towards FOH in flow cells as red squares. Unfortunately, to our knowledge there are no published results of electrocatalytic hydrogenation of furfural to 2MF in flow cells. Still, as a point of reference, state-of-the-art results obtained in the H-cell allowed for furfural conversion to 2MF with a FE of 60% at current densities of 200 mA cm^{-2}.[68] The work of Yao *et al.* is also noteworthy as they reported the stable production of furfuryl alcohol in a flow cell system for 20 hours at 0.1 A cm^{-2} at 97% FE, reaching an economic breakeven point.[70] Unfortunately, the full cell potential was not reported. We believe that accessing *zones A* and *B* with furfural ECH devices is realistic based on state-of-the-art lab-scale results and also when compared, for example, with performance metrics of CO_2 electrolysers at +50% market premium (2.47–2.75 V, 87–93% FE).[229]

Now that we have defined an accessible range of operation where furfural ECH is attractive from an energy intensity point of view, we aim to evaluate the economic costs associated with a hypothetic electrolyser converting furfural to FOH (resp. 2MF) at a cell potential of 2.1 V (resp. 2.3 V) at 94% FE_{FOH} (resp. 90% FE_{2MF}). In light of the above efficiency analysis, the energy intensity of these processes would be 4.38 GJ t_{FOH}^{-1} and 12 GJ t_{2MF}^{-1}. Three different models are evaluated for an electrochemical plant converting furfural (see Fig. 8):

Case 1: PV-fed only (at an optimal scaling factor)

Case 2:: hybrid plant mixing grid and PV

Case 3: grid electricity only

The capacity of the plant to sell electricity to the grid is not considered here. The parameters used in the different **cases** are displayed in Table S2.† A fourth case (**4**) consisting of an electrolyser producing H_2 for a thermocatalytic reactor was also used as a reference (as it currently corresponds to the most represented approach towards defossilized biorefineries). In this case, conversion costs were approximated by the sum of the hydrogen production costs (6–9 \$ per kg_{H_2})[230] and reactor costs (46.5 \$ per $t_{FOH/2MF}$). The reactor costs were estimated using the results from two recent techno-economic analyses (see ESI†).[231,232] We deem the added costs of pressurizing and heating the reactor to be negligible compared with these two contributions on the basis of a cost breakdown analysis from Li *et al.*[231] For biomass electrolysers (**cases 1, 2 and 3**), current densities above 300 mA cm^{-2} are considered. This is because the majority of cost reductions associated with scaling (mainly from decreased electrode surface area at constant output) are achieved for operating current densities of 300–500 mA cm^{-2}, as shown in various techno-economic studies.[233,234] When such currents are attained during long-term operation (>100–1000 hours stability for laboratory systems), the remaining economic gains then usually come from improved energy efficiency (increased FE or decreased cell voltage). Importantly, to date, the reported current densities and stability for both considered electrochemical hydrogenation reactions still fall short of these values, highlighting the importance of reaching this milestone to consider a potential technology transfer. We also note that reaching 300 mA cm^{-2} should be compatible with the target cell voltages of 2.1 V and 2.3 V for FOH and 2MF respectively (see Fig. 7b).

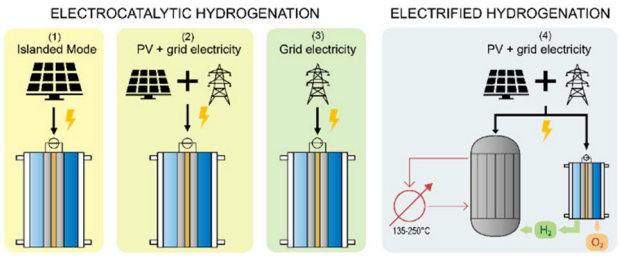

Fig. 8 Illustration of the different operation modes considered in the cost calculations study.

Moreover, as furfural is the main feedstock in this process, its own price is an important driver of the product price.[232] However, the literature is relatively imprecise regarding the furfural price per kg, ranging from 1 to 2 $ per kg.[224,232,235] Thus, due to this uncertainty, the analysis will be focused on the conversion cost and not the final product cost.

On this basis, the levelized conversion cost (LCC) of furfural to FOH or 2MF can be calculated as the sum of the annual capital expenditure (CAPEX), operating expenditure (OPEX, as a percentage of CAPEX per year), total electricity consumption of 1 kW of electrolyser in a year E and electricity price P with regards to $\dot{m}$, the mass of product a kW of electrolyser can produce throughout its operation time:

$$\mathrm{LCC}\,[\$\,per\,\mathrm{t}] = \frac{(\mathrm{AF}+\mathrm{OPEX})\,[\mathrm{year}^{-1}]\cdot \mathrm{CAPEX}\,[\$\,per\,\mathrm{kW}] + E\,[\mathrm{kWh\,per\,kW\,per\,year}]\cdot P\,[\$\,per\,\mathrm{kWh}]}{\dot{m}_{\mathrm{FOH,2MF}}\,[\mathrm{t\,per\,kW\,per\,year}]} \quad (6)$$

where AF is the annuity factor:

$$\mathrm{AF} = \frac{r(1+r)^n}{(1+r)^n - 1} \quad (7)$$

with r the discount rate (%) and n the electrolyser lifetime (year). Moreover $\dot{m}_{\mathrm{FOH,2MF}}$ is the annual product output per kW of electrolyser:

$$\dot{m}_{\mathrm{FOH,2MF}}\,[\mathrm{t\,per\,kW\,per\,year}] = \frac{E\,[\mathrm{GJ\,per\,kW\,per\,year}]}{\mathrm{EI}\,[\mathrm{GJ\,t}^{-1}]} \quad (8)$$

where E is the electricity consumed by a kW of electrolyser in a year from solar PV or grid, and EI is the previously calculated energy intensity for the synthesis of the product. Our results are presented in Fig. 9. They show that operating a plant supplied by PV disconnected from the grid (**case 1**) results in the highest cost of conversion of furfural to either FOH or 2MF (112–197 $ per t_{FOH}; 306–541 $ per t_{2MF}). Other studies have shown that the optimal scaling factor of the electrolyser for this mode of operation (islanded PV) was around 60% of the PV plant capacity (*i.e.* 0.6 kW of electrolyser per kW of installed PV).[236,237] This configuration results in a higher utilization rate of the electrolyser but also increases the amount of curtailed electricity (around 25%).[238] The consequence of this scaling factor is an increased PV LCOE from the plant point of view, and therefore a higher conversion cost. In addition, the electrolyser cannot operate during night-time, reducing the electrolyser use factor. These considerations explain the high conversion costs associated with this scenario. A straightforward way to bring the curtailment rate to zero and increase the use rate is to connect the plant to the electrical grid (**case 2**). In this fashion, grid electricity can compensate for PV during low production times and the electrolyser capacity can be scaled at 100% of PV power. As a result, conversion costs in this configuration are calculated to be generally lower than in **case 1:** 84–122 $ per t_{FOH} and 230–335 $ per t_{2MF}. Here, PV allows the supply of 24% of the electricity needs of the electrolyser at low electricity cost while grid electricity, even if at a

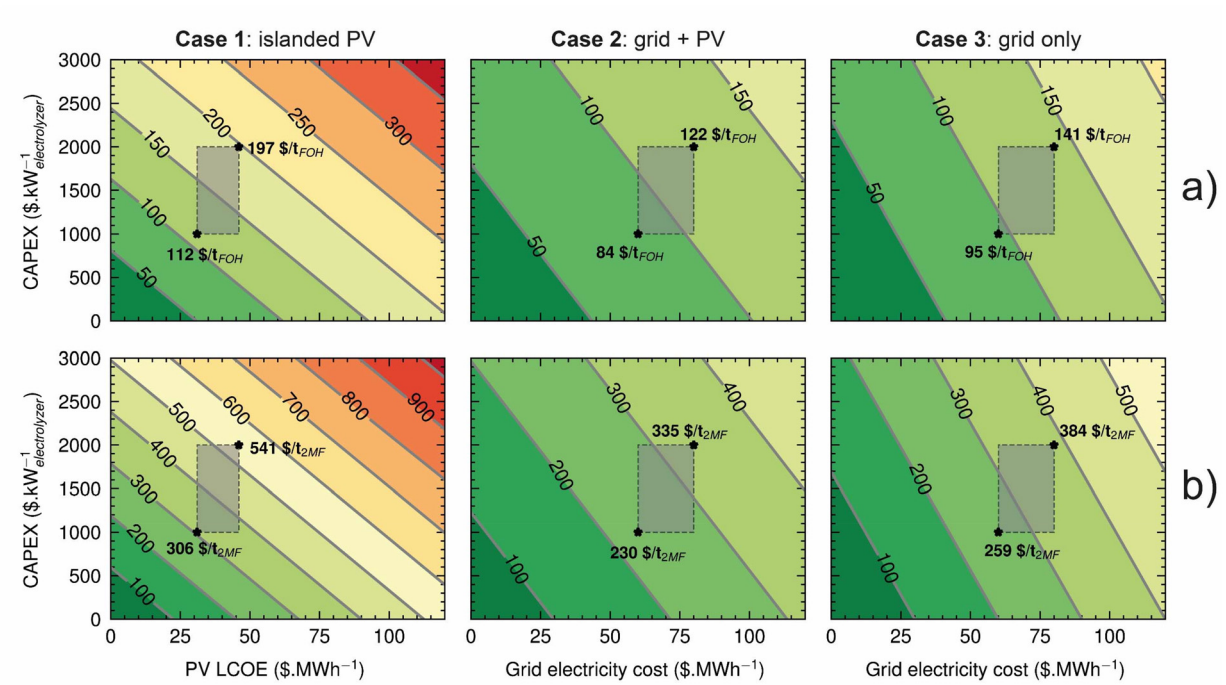

Fig. 9 Contour plot of the conversion costs of furfural to furfuryl alcohol (a) and 2-methylfuran (b) as a function of electricity cost and electrolyser CAPEX for **cases 1, 2 and 3**.

higher price, allows an increase in the electrolyser use rate during low production times. Finally, the plant can also be operated while only being connected to the grid (**case 3**). The advantages of this approach are the reduction of the initial investment cost, since no PV plant must be installed, eased construction process and less surface requirement. However, grid electricity is notably costlier than utility-scale PV and prices of 60–80 $ per MWh can be expected. In addition, the carbon content of grid electricity is still high in most countries: 244 g_{CO_2} kWh^{-1} in EU27 and 390 g_{CO_2} kWh^{-1} in the US.[239] Our model estimates the associated conversion costs to be in the range of 95–141 $ per t_{FOH} and 259–384 $ per t_{2MF}, which is *ca.* 15% more than the PV + grid case (**case 2**). These estimations confirm the economic and environmental advantages of using PV as a source of electricity in tandem with the grid (in the form of a Price Purchase Agreement, or direct feed). Interestingly, while the islanded PV + electrolyser concept offers the lowest amount of CO_2 emissions, it is evaluated to be the most expensive option, due to intermittency and scaling factor issues. Furthermore, accelerated degradation and lower energy efficiency were observed in equivalent variable energy-fed systems, which further hinders the long-term competitivity of our **case 1**.[240–242] Overall, those preliminary results are in line with the trend observed in water electrolysis studies, where off-grid configurations are costlier,[238] and a mixed PV + grid approach currently offers the best trade-off in conversion costs and CO_2 emissions. As a matter of comparison, we note that Han *et al.* estimated a lower cost for electrochemical hydrogenation of furfural to furfuryl alcohol at 55.74 $ per t_{FOH} (without purification costs).[69] Most of the price difference lies in their choice of parameters: 30 $ per MWh and 275.55 $ per $kW_{electrolyser}$ (*vs.* 60–80 $ per MWh and 1000–2000 $ per $kW_{electrolyser}$ in our model).

Then, we address the environmental benefits (in terms of CO_2 emissions) and the associated costs of using ECH compared with established thermocatalytic hydrogenation processes. For the latter, hydrogenation costs are taken as the sum of H_2 production costs by steam methane reforming (SMR) (2 $ per kg_{H_2}) added to the reactor cost (46.5 $ per $t_{FOH/2MF}$). The results of our analysis are presented in Fig. 10. We find that only the islanded PV plant can achieve some level of decarbonization compared with SMR H_2 while the other solutions would actually emit more CO_2 during operation considering the current high CO_2 intensity of the EU27 electrical grid (Fig. 10b). However, using islanded PV to reduce CO_2 emissions comes at the expense of generating the highest conversion costs of all the scenarios explored here (Fig. 9a). As such, our results drive us to advocate for the rapid and continuous integration of low-carbon electricity sources, and especially PV with battery storage, in the electricity production mix to allow for chemical industry decarbonation and defossilization. Importantly, in some countries such as Sweden, Switzerland and France, or regions like Québec and Nordeste, electricity carbon intensity already sits below 50 g_{CO_2} kWh^{-1}. Performing furfural ECH with this carbon intensity would reduce the CO_2 emissions of the conversion process by at least two thirds (low-carbon grid case in Fig. 10b and e). In this case, the corresponding CO_2 abatement costs for **cases 1 to 4** are displayed in Fig. 10c and f. In those nations and regions, we find that the lowest carbon abatement cost for FOH and 2MF synthesis is constituted by a mix of direct PV feed and low-carbon grid electricity. This cost is evaluated to range from −27 to 265 $ per t_{CO_2} and from 293 to 653 $ per t_{CO_2} for FOH and 2MF, respectively. For context, the EU Emissions Trading System, one of the most stringent and comprehensive carbon pricing systems, reached an all-time high of 100 $ t_{CO_2} in 2023. We estimate that abatement costs for 2MF synthesis in **case 2** (PV + grid) could be met around 2040–2050 when using the median 5.70% carbon price growth rate Gollier collected in the IPCC database of 767 integrated assessment models.[243] In an attempt to estimate a cost-efficient carbon price, Gollier also proposed an optimal carbon price of 213.5 and 362.3 $ per t_{CO_2} for the 2021–2035 and 2036–2050 periods, which are displayed in Fig. 8c and f. Interestingly, in the most optimistic, yet realistic, scenario for furfural ECH to FOH conversion (1000 $ per $kW_{electrolyser}$ and 60/31 $ per $MWh_{grid/solar}$), CO_2 abatement costs can even be negative. It means the conversion step can cost less than it currently does by fossil-based means while emitting 70% less CO_2 (electricity from a low carbon grid; 55 *vs.* 185 kg_{CO_2} t_{FOH}). We note that, on average, the abatement costs we calculated for FOH synthesis in **case 2** are relatively low for an industrial process, making it appealing to demonstrate the feasibility of biomass electrocatalytic valorisation at medium-scale. We estimate that adopting a PV + grid configuration (**case 2**) allows a significant reduction in CO_2 emissions from 441 to 149 kg_{CO_2} $t_{2MF}{}^{-1}$ (14.1 to 4.8 g_{CO_2} MJ^{-1}) compared with fossil-based H_2 hydrogenation. Finally, we find that 2MF synthesis through ECH (**case 2**) is a preferable approach to reduce CO_2 emissions compared with the reference electrified hydrogenation scenario (**case 4**, 630–1102 $ per t_{CO_2}) thanks, in part, to a lower initial CAPEX: an electrified hydrogenation supplied by green H_2 requires an initial investment for an electrolyser and a reactor, while only an electrolyser is necessary in the case of ECH. We note that the CO_2 abatement costs for **case 4**, while being high, generally agree with recent literature on chemical and heavy industry decarbonization using H_2-based technologies.[244]

Therefore, in light of this case study, the direct electrochemical conversion of bio-based molecules seems to be a preferable alternative to indirect defossilization through electrolytic H_2. Still, further cost and CO_2 emissions reductions of grid electricity are required to globally achieve an ecologically and economically sustainable electrochemical valorisation of bio-based feedstock. In this sense, PV plays a role for the development of electrified biorefinery as a cheap and rapidly scalable carbon-free electricity source but also as a means to decarbonize grid electricity. Our study remains preliminary and aims to serve more detailed studies and techno-economic analyses aiming at estimating rigorously the costs of biomass electrochemical hydrogenation (by considering labour costs, taxes, grid fees, separation costs and other hidden costs). Finally, as highlighted previously, electrochemical systems

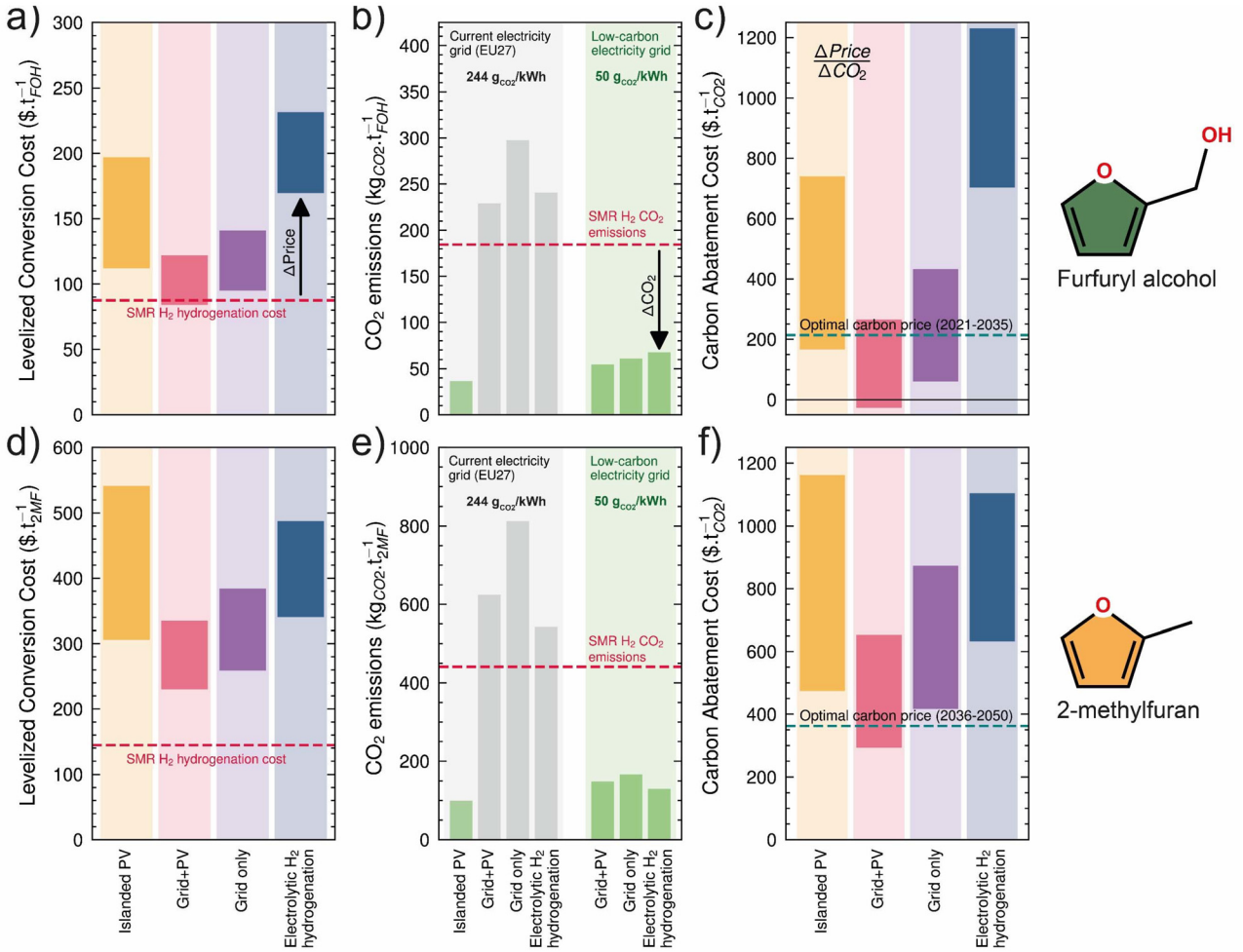

Fig. 10 Levelized conversion cost of furfural to FOH (a) and 2MF (d) compared with SMR H_2 hydrogenation. CO_2 emissions associated with ECH when electricity originates from current grid electricity (EU27) or low-carbon grid in the case of FOH (b) or 2MF (e) synthesis. CO_2 abatement costs of switching thermocatalytic hydrogenation of furfural to ECH of furfural for **cases 1, 2, 3 and 4** in the case of FOH (c) and 2MF synthesis (f).

converting biomass-based molecules are still scarce in the literature and more research is required to demonstrate convincing lab prototypes and bring the technology to higher TRL. Still, rapid and accelerating recent progress on this front gives hope for a successful technology transfer in the relatively short term.

4. Outlook: combining oxidation and reduction valorisation processes

The previous section highlighted the economic advantage of furfural ECH *versus* electrified hydrogenation with electrolytic H_2. However, higher costs than those of the fossil-based processes are still observed. Generally speaking, commodities production through electrochemical processes (*e.g.* water electrolysis) face high production costs and lack of competitivity against fossil-based technologies. Those high costs partly originate from the high energy demand induced by the oxygen evolution reaction at the anode for commonly proposed electrolyser designs. With a standard potential of 1.23 V_{RHE} and an overpotential above 200 mV in acidic and alkaline conditions, much of the electrical energy is dedicated to producing O_2, a low-value chemical. Biomass, on the other hand, is composed of molecules with low thermodynamic oxidation potentials, as highlighted in Fig. 4. Thus, there is, in theory, a strong interest in coupling reduction reactions (HER, CO_2RR, ECH, direct iron ore reduction...) with a thermodynamically easy and valuable anodic reaction (HMF oxidation, glucose oxidation, furfural oxidation...). The expected result is a lowered cell potential at similar current densities combined with the synthesis of a valuable product at the cathode. Examples of such processes where alternative oxidation reactions were used to replace the OER are provided in Table 1. This strategy, when combined with optimized electrocatalysts, could in fact result in much lowered operating cell potentials: below 1.5 V or even below 1.0

V in some cases. However, it is important to note that, in some cases the valuable aspect of the molecule has to be put in perspective with the limited market size. For example, in the biofuel sector, overproduction of glycerol (co-product of biodiesel) led its price to drop as demand could not keep up.[245,246] For the proposed solar-driven processes, the reaction choice is important to avoid creating overcapacities, saturating a market and reducing the income of the biorefinery. HMFOR is a straightforward reaction to consider and has been the object of many recent studies (see section 2).[235] One HMF oxidation product in particular, FDCA, has the potential to compete with fossil-based terephthalic acid to produce bio-based plastics while reducing the associated CO_2 emissions by 35–50%.[247,248] The aimed-for market is over the Mt per year scale and the economic advantages of HMFOR have been demonstrated in recent research articles.[146,249]

Furthermore, inside an integrated biorefinery, point-source CO_2 emissions may also remain due to the demand for heating (biomass waste, bio-gas or fossil gas can be used as fuels) or stoichiometric emissions from specific biorefinery processes. In this context, the emitted CO_2 could be captured and valorised through a reduction reaction, for instance into ethylene or methanol. We note here that lowering the operating voltage of CO_2RR electrolysers by more than 0.4 V would enable the economic viability of using acidic conditions and thus mitigate carbonate crossover, and lowering it by 1 V could enable the use of bipolar membranes, potentially resulting in significant improvements in long-term device stability.[250] In this context, coupling CO_2RR with the oxidative valorisation of biomass-derived molecules appears interesting. Then, CO_2RR products such as ethylene or methanol can be oxidized downstream to contribute to the current Mt per year industrial production of ethylene oxide/ethylene glycol or formaldehyde respectively. Those oxidation reactions can be paired with reduction reactions (*e.g.* HER to provide cheaper H_2 to the hydrogenation processes while delivering valuable commodities at the anode).[251,252] On a broader basis, the electrooxidation of some alcohols into aldehydes/ketones or carboxylic acid can lead to valuable molecules (*e.g.* ethanol to acetaldehyde).[253,254] These two examples illustrate opportunities specific to solar-driven electrochemical transformation and eventually photoelectrochemical transformations, where an oxidation process must be coupled to a reduction process, and where these two half-processes can be driven in separate physical locations, separated by a membrane if needed. Therefore, in addition to possible gains in energy efficiency, product selectivity or operation under greener chemical conditions, introducing electrochemical approaches in biorefineries also unlocks novel integration strategies where two valorisation processes can be synergistically combined.

With this in mind, a snapshot of a possible model of integrated biorefinery taking advantage of paired electrolysis and common chemical processes is displayed in Fig. 11. Briefly, the biorefinery consists of fractionation/hydrolysis/dehydration units producing furfural and HMF from hemi-cellulose and cellulose. Lignin can be recovered as well and valorised into cycloalkanes for SAF.[255–257] Furfural and HMF are electrochemically upgraded in 2-methylfuran and HMF, respectively.[101,258,267] 2-MF follows hydroxyalkylation with acetaldehyde (produced from bio-ethanol) and subsequently HDO to produce C10–C16 fuels, as described in the so-called Sylvan process.[46] The heat required by the different units is produced by oxyfuel combustion of gas or waste, with O_2 originating from CO_2RR and furfural ECH processes. Oxyfuel combustion allows for enhanced CO_2 capture,[259] which is then valorised into ethylene through the CO_2RR. Ethylene electrochemical oxidation leads to the production of ethylene glycol along with H_2.[260–262] Ethylene glycol can polymerize with FDCA into PEF,

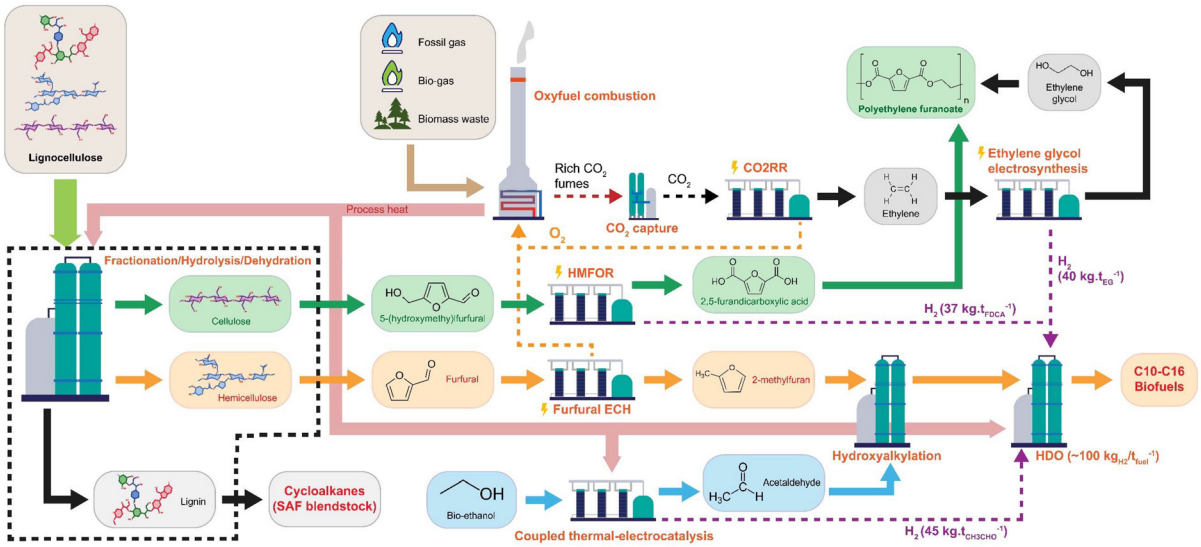

Fig. 11 Overview of a conceptual electrified biorefinery flow diagram using currently investigated processes.

a polymer analogous to PET.[263] HMFOR and ethylene glycol synthesis provide the required H_2 for the HDO step producing the biofuels. Different processes can be considered: ethylene can be produced through a direct CO_2RR or tandem CO_2RR (CO_2-to-CO followed by CORR) for example.[264] Those engineering choices depend on technology development in the near future. The described hypothetical plant aims to demonstrate the relevance and synergies of electrochemical processes in a biorefinery. Eerhart *et al.* investigated the technical and economic aspects of a furan biorefinery using classic thermocatalytic processes.[246,265] Their results showed beneficial aspects of upgrading both FDCA and furfural into plastics and fuels from the same feedstock and the necessity of building large plants to economically challenge fossil-based molecules. However, the larger the biorefinery, the higher the cost of feedstock and the CO_2 emissions associated with transport. Thanks to their modularity, biomass electrolysers could allow the downscaling of those refineries to sizes more aligned with feedstock availability. For example, recent studies on ethylene production by a CO_2RR showed that a minimum of 3 $kt_{C_2H_4}$ per year plant is sufficient to achieve economies of scale for the upstream and downstream processes.[266] Still, the development of solar-powered biomass conversion systems from laboratory to industrial scale requires important additional research efforts. While some systems display appreciable activity and selectivity, their long-term stability remains unclear. Loss of activity and poisoning of catalysts are an important issue that can hinder further development.

Furthermore, to help bridge the TRL gap faster, the competitive development of solar-powered biorefineries could be promoted by policy makers, capitalizing on lessons learned from the bio-methane and bio-ethanol industries, with industrial policies such as:

- The introduction of new blending mandates of chemicals from lignocellulosic biorefineries into products or fuels
- Targeted subsidies: tax credit or direct subsidy to the end-user of chemicals
- The reduction of taxes on electricity and grid fees to ensure competitiveness of electricity price and fairness of effective tax rates between energies
- Access to credit and loan guarantees to solar-powered biorefinery projects.

Another critical aspect of the overview proposed in Fig. 11 is the mismatch in the current production scale and demand between biomass-derived compounds and high-tonnage commodity chemicals, such as ethylene (between a few hundreds of kt per year and several hundreds of Mt per year). Designing the integration of these different processes inside a coherent innovative model of solar-powered refinery will thus necessitate an important research effort to demonstrate the scalability, versatility and viability of electrocatalytic or photoelectrochemical approaches in this range of operation. While several authors have started to explore this topic in recent years, we believe that including this long-term goal more systematically in the design and choice of (photo) electrochemical systems of interest would greatly benefit progress towards a cohesive technological landscape for a solar-powered chemical industry.

5. Conclusion

In this critical review, we proposed an overview of the current state-of-the art approaches that could be involved in solar lignocellulose biorefinery concepts. We show that solar-driven electrocatalytic conversions and photoelectrochemical approaches have reached important milestones at the lab scale but the benefit of their implementation at an industrial level remains uncertain. In particular, photoelectrochemical processes remain quite far from industrial relevance, but the advantages of using biomass resources and generating value-added products has a chance to improve the relevance of this approach compared with its current prospective applications in solar hydrogen production. To partly answer whether these new approaches are relevant at all, we proposed a preliminary comparative assessment of the energy, economics and emissions involved in furfural hydrogenation by carbon-neutral thermocatalytic and electrocatalytic processes. We found that electrocatalytic strategies are pertinent and can be competitive at the industrial scale, provided there is a good enough selectivity. We show that while powering the electrolyser with islanded PV provides the lowest carbon footprint, operating costs are too high for it to be viable. Instead, a "grid + PV" approach appears to be more reasonable in the short term, even reaching negative carbon abatement costs in best case scenarios. Finally, we emphasize that involving electrochemical, and eventually photochemical/photoelectrochemical, processes in future biorefineries could unlock completely new value chains compared with the legacy petrochemical sector, due to the specificity of their respective operating conditions. While it would be illusory and counterproductive to replace all the thermocatalytic processes in current biorefinery models, we argue that electrocatalysis can have an attractive and important role to play even in the short term for industrial lignocellulose valorisation strategies, especially if combined with other waste resources valorisation (*e.g.* CO_2). Importantly, the case study performed here concerns the valorisation of furfural, a molecule produced on a large scale for a biomass-derived chemical. However, it is important to consider that converting the entire annual furfural production to FOH or 2MF electrochemically would "only" require 50 MW of biomass electrolyser capacity, far below the scale required for the defossilization of the production of the largest chemical markets of commodity chemicals and fuels. Therefore, while direct electrification appears sensible for medium-scale value chains, a different analysis is required to study the replacement of the largest sectors of the thermocatalytic petrochemical industry. Finally, to confirm the validity of our analysis, more studies performed at industrially-relevant current densities, cell voltages, and cell dimensions are urgently required. We also believe that developing advanced materials and systems specifically designed around biomass valorisation,

rather than merely transferring elements developed for previous applications (typically water splitting), would be highly beneficial. Thankfully, recent trends in publications in the field tend to indicate that an increasing number of researchers are currently interested in tackling this challenging task, and there is little doubt that solar-driven lignocellulose valorisation will know exciting progress in the near future.

Author contributions

CS participated in the conceptualization, data curation, methodology and writing of the manuscript, CH participated in data curation and writing of the manuscript, and MSP participated in conceptualization, methodology, data curation, project administration, funding acquisition, supervision and writing of the manuscript.

Conflicts of interest

The authors declare no conflict of interest.

List of acronyms

2-MeTHF	2-Methyltetrahydrofuran
2MF	2-Methylfuran
ACT	4-Acetamido-TEMPO
BHMF	2,5-Bis(hydroxymethyl)furan
BTX	Benzene–toluene–xylene
CAPEX	Capital expenditure
CO_2RR	Electrochemical CO_2 reduction reaction
DFF	Diformylfuran
ECH	Electrochemical hydrogenation
EU27	27 member-states of the European Union
FDCA	Furandicarboxylic acid
FE	Faradaic efficiency
FFCA	5-Formyl-2-furoic acid
FOH	Furfuryl alcohol
HDO	Hydrodeoxygenation
HER	Hydrogen evolution reaction
HMF	5-Hydroxymethylfurfural
HMFCA	5-Hydroxymethl-2-furoic acid
HMFOR	Electrochemical HMF oxidation reaction
KABNO	9-Azabicyclo[3,3,1]nonan-3-one-9-oxyl
LCOE	Levelized cost of electricity
OER	Oxygen evolution reaction
OPEX	Operational expenditure
PCET	Proton-coupled electron transfer
PEC	Photoelectrochemical
PEF	Polyethylene furoate
PET	Polyethylene terephthalate
PINO	Phthalimide-*N*-oxyl
PMA	Phosphomolybdic acid
PV	Photovoltaic
RHE	Reversible hydrogen electrode
SAF	Sustainable aviation fuel
SCLJ	Semiconductor–liquid junction
SMR	Steam methane reforming
TEMPO	2,2,6,6-Tetramethyl-1-piperidine *N*-oxyl
THFA	Tetrahydrofurfuryl alcohol
TRL	Technology readiness level

Data availability

All original data are directly provided in the manuscript and ESI.†

Acknowledgements

The authors are grateful to the Agence Nationale de la Recherche (ANR) through the project MEGOPE (ANR-22-CE29-0015), and the Doctoral School of Université Claude Bernard Lyon 1, who provided the salaries of CS and CH respectively.

References

1 K. Richardson, W. Steffen, W. Lucht, J. Bendtsen, S. E. Cornell, J. F. Donges, M. Drüke, I. Fetzer, G. Bala, W. von Bloh, G. Feulner, S. Fiedler, D. Gerten, T. Gleeson, M. Hofmann, W. Huiskamp, M. Kummu, C. Mohan, D. Nogués-Bravo, S. Petri, M. Porkka, S. Rahmstorf, S. Schaphoff, K. Thonicke, A. Tobian, V. Virkki, L. Wang-Erlandsson, L. Weber and J. Rockström, *Sci. Adv.*, 2023, **9**, eadh2458.
2 M. S. Prévot, V. Finelli, X. Carrier, G. Deplano, M. Cavallo, E. A. Quadrelli, J. Michel, M.-H. Pietraru, C. Camp, G. Forghieri, A. Gagliardi, S. Seidel, A. Missemer, B. Reuillard, B. Centrella, S. Bordiga, M. G. S. González, V. Artero, K. V. A. Birkelbach and N. von Wolff, *Chem. Sci.*, 2024, **15**, 9054–9086.
3 Z. Liu, K. Wang, Y. Chen, T. Tan and J. Nielsen, *Nat. Catal.*, 2020, **3**, 274–288.
4 D. Pérez-Almada, Á. Galán-Martín, M. M. Contreras and E. Castro, *Sustainable Energy Fuels*, 2023, **7**, 4031–4050.
5 N. Dahmen, I. Lewandowski, S. Zibek and A. Weidtmann, *GCB Bioenergy*, 2019, **11**, 107–117.
6 B. B. Hewetson, X. Zhang and N. S. Mosier, *Energy Fuels*, 2016, **30**, 9975–9977.
7 G. Tofani, E. Jasiukaitytė-Grojzdek, M. Grilc and B. Likozar, *Green Chem.*, 2024, **26**, 186–201.
8 Y. Liu, N. Deak, Z. Wang, H. Yu, L. Hameleers, E. Jurak, P. J. Deuss and K. Barta, *Nat. Commun.*, 2021, **12**, 5424.
9 Y. Bao, Y. Wang, C. Yan and Z. Xue, *Green Chem. Eng.*, 2025, **6**, 21–35.
10 M. Zhou, O. A. Fakayode, A. E. A. Yagoub, Q. Ji and C. Zhou, *Renewable Sustainable Energy Rev.*, 2022, **156**, 111986.

11 M. Jin, P. J. Slininger, B. S. Dien, S. Waghmode, B. R. Moser, A. Orjuela, L. da C. Sousa and V. Balan, *Trends Biotechnol.*, 2015, **33**, 43–54.
12 J. Rajesh Banu, M. Preethi, S. Kavitha, V. K. Tyagi, M. Gunasekaran, O. P. Karthikeyan and G. Kumar, *Fuel*, 2021, **302**, 121086.
13 J. Zakzeski, P. C. A. Bruijnincx, A. L. Jongerius and B. M. Weckhuysen, *Chem. Rev.*, 2010, **110**, 3552–3599.
14 R. Rinaldi, R. Jastrzebski, M. T. Clough, J. Ralph, M. Kennema, P. C. A. Bruijnincx and B. M. Weckhuysen, *Angew. Chem., Int. Ed.*, 2016, **55**, 8164–8215.
15 M. V. Galkin and J. S. M. Samec, *ChemSusChem*, 2016, **9**, 1544–1558.
16 K. Huang, P. Fasahati and C. T. Maravelias, *iScience*, 2020, **23**, 100751.
17 R. J. Khan, C. Y. Lau, J. Guan, C. H. Lam, J. Zhao, Y. Ji, H. Wang, J. Xu, D.-J. Lee and S.-Y. Leu, *Bioresour. Technol.*, 2022, **346**, 126419.
18 Z.-M. Xu, J.-Y. Luo and Y.-B. Huang, *Green Chem.*, 2022, **24**, 3895–3921.
19 S. Wang, A. Cheng, F. Liu, J. Zhang, T. Xia, X. Zeng, W. Fan and Y. Zhang, *Ind. Chem. Mater.*, 2023, **1**, 188–206.
20 Y. Wu, H. Wang, J. Peng and M. Ding, *Catal. Today*, 2023, **408**, 92–110.
21 F. Güleç, A. Parthiban, G. C. Umenweke, U. Musa, O. Williams, Y. Mortezaei, H. Suk-Oh, E. Lester, C. C. Ogbaga, B. Gunes and J. A. Okolie, *Biofuels, Bioprod. Biorefin.*, 2024, **18**, 755–781.
22 L. Qu, X. Jiang, Z. Zhang, X. Zhang, G. Song, H. Wang, Y. Yuan and Y. Chang, *Green Chem.*, 2021, **23**, 9348–9376.
23 P. He, L. Li, Y. Shao, Q. Yi, Z. Liu, H. Geng, Y. Liu and V. Valtchev, *ChemCatChem*, 2024, **16**, e202301681.
24 X. Zhang, K. Wilson and A. F. Lee, *Chem. Rev.*, 2016, **116**, 12328–12368.
25 B. Kusserow, S. Schimpf and P. Claus, *Adv. Synth. Catal.*, 2003, **345**, 289–299.
26 B. García, A. Orozco-Saumell, M. López Granados, J. Moreno and J. Iglesias, *ACS Sustainable Chem. Eng.*, 2021, **9**, 14857–14867.
27 T. N. Dharmapriya and P.-J. Huang, *J. Taiwan Inst. Chem. Eng.*, 2024, **162**, 105585.
28 Z. Wang, S. Xia, X. Wang, Y. Fan, K. Zhao, S. Wang, Z. Zhao and A. Zheng, *Renewable Sustainable Energy Rev.*, 2024, **196**, 114332.
29 P. Zhao, Y. Zhang, Y. Wang, H. Cui, F. Song, X. Sun and L. Zhang, *Green Chem.*, 2018, **20**, 1551–1559.
30 K. Wang, A. Rezayan, L. Si, Y. Zhang, R. Nie, T. Lu, J. Wang and C. Xu, *ACS Sustainable Chem. Eng.*, 2021, **9**, 11351–11360.
31 Y. Wang, X. Yuan, J. Liu and X. Jia, *ChemPlusChem*, 2024, **89**, e202300399.
32 J. E. Romo, N. V. Bollar, C. J. Zimmermann and S. G. Wettstein, *ChemCatChem*, 2018, **10**, 4805–4816.
33 J. Esteban, A. J. Vorholt and W. Leitner, *Green Chem.*, 2020, **22**, 2097–2128.
34 L. Zhu, X. Fu, Y. Hu and C. Hu, *ChemSusChem*, 2020, **13**, 4812–4832.
35 T. Cai, C. Liu, J. Jiang, X. Meng, A. J. Ragauskas and K. Wang, *Trends in Chemistry*, 2024, **6**, 219–233.
36 Z. Zhang and G. W. Huber, *Chem. Soc. Rev.*, 2018, **47**, 1351–1390.
37 Q. Zhang, Z. Wan, I. K. M. Yu and D. C. W. Tsang, *J. Cleaner Prod.*, 2021, **312**, 127745.
38 J. V. Machado, M. L. A. da Silva, C. L. S. Silva, M. C. G. Correia, A. D. da Silva Ruy and L. A. M. Pontes, *Catal. Commun.*, 2023, **182**, 106740.
39 S. T. Al-Absi, K. Bashir, M. Abbotsi-Dogbey, Q. Zhang, D. Zhang, J. Liu, A. Mohamed, M. Yassien, W. Yan and X. Jin, *Ind. Eng. Chem. Res.*, 2025, **64**, 10101–10116.
40 D. Zhao, T. Su, Y. Wang, R. S. Varma and C. Len, *Mol. Catal.*, 2020, **495**, 111133.
41 D. J. Aranha and P. R. Gogate, *Ind. Eng. Chem. Res.*, 2023, **62**, 3053–3078.
42 C. Chen, M. Lv, H. Hu, L. Huai, B. Zhu, S. Fan, Q. Wang and J. Zhang, *Adv. Mater.*, 2024, **36**, 2311464.
43 J. M. Molinaro, J. Swartzentruber, V. W. Ledger, Z. T. Fredericks, D. M. Alonso and S. G. Wettstein, *EES Catal.*, 2025, **3**, 595–620.
44 K. Zhao, B. Wen, Q. Tang, F. Wang, X. Liu, Q. Xu and D. Yin, *Green Chem.*, 2024, **26**, 9957–9992.
45 M. Thewes, M. Muether, S. Pischinger, M. Budde, A. Brunn, A. Sehr, P. Adomeit and J. Klankermayer, *Energy Fuels*, 2011, **25**, 5549–5561.
46 A. Corma, O. De La Torre and M. Renz, *Energy Environ. Sci.*, 2012, **5**, 6328.
47 W. Zhang, S. Ma and J.-H. Yang, *ChemistrySelect*, 2024, **9**, e202401310.
48 A. Racha, C. Samanta, S. Sreekantan and B. Marimuthu, *Energy Fuels*, 2023, **37**, 11475–11496.
49 A. Tuan Hoang and V. Viet Pham, *Renewable Sustainable Energy Rev.*, 2021, **148**, 111265.
50 D. Banerjee, A. K. Sahu, J. K. Clegg and S. Upadhyayula, *Chem. Eng. J.*, 2024, **493**, 152552.
51 Y. Zhang, H. Cui and H. Xia, *ChemSusChem*, 2025, **18**, e202401390.
52 L. Hong, H. Zhang, L. Hu, R. Xiao and S. Chu, *Sci. Adv.*, 2024, **10**, eadn9441.
53 S. Jung and E. J. Biddinger, *Energy Technol.*, 2018, **6**, 1370–1379.
54 Y. Cao and T. Noël, *Org. Process Res. Dev.*, 2019, **23**, 403–408.
55 S. Jung, A. N. Karaiskakis and E. J. Biddinger, *Catal. Today*, 2019, **323**, 26–34.
56 J. Anibal and B. Xu, *ACS Catal.*, 2020, **10**, 11643–11653.
57 A. S. May and E. J. Biddinger, *ACS Catal.*, 2020, **10**, 3212–3221.
58 R. J. Dixit, K. Bhattacharyya, V. K. Ramani and S. Basu, *Green Chem.*, 2021, **23**, 4201–4212.
59 P. Zhou, Y. Chen, P. Luan, X. Zhang, Z. Yuan, S.-X. Guo, Q. Gu, B. Johannessen, M. Mollah, A. L. Chaffee,

D. R. Turner and J. Zhang, *Green Chem.*, 2021, **23**, 3028–3038.
60 A. S. May, S. M. Watt and E. J. Biddinger, *React. Chem. Eng.*, 2021, **6**, 2075–2086.
61 S. Liu, N. Govindarajan and K. Chan, *ACS Catal.*, 2022, **12**, 12902–12910.
62 Z. Xia, Y. Li, J. Wu, Y.-C. Huang, W. Zhao, Y. Lu, Y. Pan, X. Yue, Y. Wang, C.-L. Dong, S. Wang and Y. Zou, *Sci. China: Chem.*, 2022, **65**, 2588–2595.
63 P. Zhou, L. Li, V. S. S. Mosali, Y. Chen, P. Luan, Q. Gu, D. R. Turner, L. Huang and J. Zhang, *Angew. Chem.*, 2022, **134**, e202117809.
64 Y. Cui, Z. Wang and S. Li, *Catal. Sci. Technol.*, 2023, **13**, 1846–1854.
65 S. Liu, Z. Mukadam, S. B. Scott, S. C. Sarma, M.-M. Titirici, K. Chan, N. Govindarajan, I. E. L. Stephens and G. Kastlunger, *EES Catal.*, 2023, **1**, 539–551.
66 H. Wen, W. Zhang, Z. Fan and Z. Chen, *ACS Catal.*, 2023, 15263–15289.
67 C. Spadetto, C. Hachemi, M. Nouaille-Degorce, L. Pendu, L. Bossert, R. Temperton, A. Shavorskiy, L. Cardenas and M. S. Prévot, *ACS Catal.*, 2024, 4489–4500.
68 K. Ji, Y. Liu, Y. Wang, K. Kong, J. Li, X. Liu and H. Duan, *J. Am. Chem. Soc.*, 2024, **146**, 11876–11886.
69 S. Han, Y. Lee, J. Woo, J. Jang, Y.-E. Sung and J. Yoon, *ACS Omega*, 2024, **9**, 26285–26292.
70 Z.-C. Yao, J. Chai, T. Tang, L. Ding, Z. Jiang, J. Fu, X. Chang, B. Xu, L. Zhang, J.-S. Hu and L.-J. Wan, *Proc. Natl. Acad. Sci. U. S. A.*, 2025, **122**, e2423542122.
71 Y. Kwon and M. T. M. Koper, *ChemSusChem*, 2013, **6**, 455–462.
72 J. Lee, S. Jung, Y. T. Kim, H. J. Kim and K.-H. Kim, *Renewable Sustainable Energy Rev.*, 2023, **181**, 113337.
73 S. Fei, J. Chen, S. Yao, G. Deng, L. Nie and Y. Kuang, *J. Solid State Electrochem.*, 2005, **9**, 498–503.
74 A. Bin Kassim, C. L. Rice and A. T. Kuhn, *J. Appl. Electrochem.*, 1981, **11**, 261–267.
75 P. N. Pintauro, D. K. Johnson, K. Park, M. M. Baizer and K. Nobe, *J. Appl. Electrochem.*, 1984, **14**, 209–220.
76 J. Lessard, G. Belot, Y. Couture, S. Desjardins and C. Roy, *Int. J. Hydrogen Energy*, 1993, **18**, 681–684.
77 S. G. Chen, T. Wen and J. H. P. Utley, *J. Appl. Electrochem.*, 1992, **22**, 43–47.
78 A. Bin Kassim, C. L. Rice and A. T. Kuhn, *J. Chem. Soc., Faraday Trans. 1*, 1981, **77**, 683.
79 Y. P. Wijaya, K. J. Smith, C. S. Kim and E. L. Gyenge, *Green Chem.*, 2020, **22**, 7233–7264.
80 S. A. Akhade, N. Singh, O. Y. Gutiérrez, J. Lopez-Ruiz, H. Wang, J. D. Holladay, Y. Liu, A. Karkamkar, R. S. Weber, A. B. Padmaperuma, M.-S. Lee, G. A. Whyatt, M. Elliott, J. E. Holladay, J. L. Male, J. A. Lercher, R. Rousseau and V.-A. Glezakou, *Chem. Rev.*, 2020, **120**, 11370–11419.
81 J. Lange, R. Price, P. M. Ayoub, J. Louis, L. Petrus, L. Clarke and H. Gosselink, *Angew. Chem., Int. Ed.*, 2010, **49**, 4479–4483.
82 R. J. M. Bisselink, M. Crockatt, M. Zijlstra, I. J. Bakker, E. Goetheer, T. M. Slaghek and D. S. van Es, *ChemElectroChem*, 2019, **6**, 3285–3290.
83 F. W. S. Lucas, Y. Fishler and A. Holewinski, *Green Chem.*, 2021, **23**, 9154–9164.
84 X. Fei, J. Wang, J. Zhu, X. Wang and X. Liu, *ACS Sustainable Chem. Eng.*, 2020, **8**, 8471–8485.
85 S. K. Burgess, J. E. Leisen, B. E. Kraftschik, C. R. Mubarak, R. M. Kriegel and W. J. Koros, *Macromolecules*, 2014, **47**, 1383–1391.
86 G. Grabowski, J. Lewkowski and R. Skowroński, *Electrochim. Acta*, 1991, **36**, 1995.
87 B. You, X. Liu, N. Jiang and Y. Sun, *J. Am. Chem. Soc.*, 2016, **138**, 13639–13646.
88 B. You, N. Jiang, X. Liu and Y. Sun, *Angew. Chem., Int. Ed.*, 2016, **55**, 9913–9917.
89 B. You, X. Liu, X. Liu and Y. Sun, *ACS Catal.*, 2017, **7**, 4564–4570.
90 S. Barwe, J. Weidner, S. Cychy, D. M. Morales, S. Dieckhöfer, D. Hiltrop, J. Masa, M. Muhler and W. Schuhmann, *Angew. Chem., Int. Ed.*, 2018, **57**, 11460–11464.
91 M. Li, L. Chen, S. Ye, G. Fan, L. Yang, X. Zhang and F. Li, *J. Mater. Chem. A*, 2019, **7**, 13695–13704.
92 N. Zhang, Y. Zou, L. Tao, W. Chen, L. Zhou, Z. Liu, B. Zhou, G. Huang, H. Lin and S. Wang, *Angew. Chem., Int. Ed.*, 2019, **58**, 15895–15903.
93 B. J. Taitt, D.-H. Nam and K.-S. Choi, *ACS Catal.*, 2019, **9**, 660–670.
94 P. Zhang, X. Sheng, X. Chen, Z. Fang, J. Jiang, M. Wang, F. Li, L. Fan, Y. Ren, B. Zhang, B. J. J. Timmer, M. S. G. Ahlquist and L. Sun, *Angew. Chem., Int. Ed.*, 2019, **58**, 9155–9159.
95 S. Choi, M. Balamurugan, K.-G. Lee, K. H. Cho, S. Park, H. Seo and K. T. Nam, *J. Phys. Chem. Lett.*, 2020, 2941–2948.
96 X. Xu, X. Song, X. Liu, H. Wang, Y. Hu, J. Xia, J. Chen, M. Shakouri, Y. Guo and Y. Wang, *ACS Sustainable Chem. Eng.*, 2022, **10**, 5538–5547.
97 Z. Li, Y. Han, B. Huang, Z. Xie and Q.-H. Wei, *Mater. Adv.*, 2023, **4**, 2449–2456.
98 Z. Yang, B. Zhang, C. Yan, Z. Xue and T. Mu, *Appl. Catal., B*, 2023, **330**, 122590.
99 I. R. Garduño-Ibarra, Z. Yan, S. A. Ebrahim, E. Baranova, J. González-Cobos, M. Prévot and P. Vernoux, *ChemElectroChem*, 2025, **12**, e202500067.
100 A. Pei, P. Wang, S. Zhang, Q. Zhang, X. Jiang, Z. Chen, W. Zhou, Q. Qin, R. Liu, R. Du, Z. Li, Y. Qiu, K. Yan, L. Gu, J. Ye, G. I. N. Waterhouse, W.-H. Huang, C.-L. Chen, Y. Zhao and G. Chen, *Nat. Commun.*, 2024, **15**, 5899.
101 L. Chen, C. Yu, X. Song, J. Dong, J. Mu and J. Qiu, *Nat. Commun.*, 2024, **15**, 8072.
102 H. Chen, J. Wang, Y. Yao, Z. Zhang, Z. Yang, J. Li, K. Chen, X. Lu, P. Ouyang and J. Fu, *ChemElectroChem*, 2019, **6**, 5797–5801.

103 N. Heidary and N. Kornienko, *Chem. Commun.*, 2019, **55**, 11996–11999.
104 D. J. Chadderdon, L. Xin, J. Qi, Y. Qiu, P. Krishna, K. L. More and W. Li, *Green Chem.*, 2014, **16**, 3778–3786.
105 R. Latsuzbaia, R. Bisselink, A. Anastasopol, H. van der Meer, R. van Heck, M. S. Yagüe, M. Zijlstra, M. Roelands, M. Crockatt, E. Goetheer and E. Giling, *J. Appl. Electrochem.*, 2018, **48**, 611–626.
106 M. Park, M. Gu and B.-S. Kim, *ACS Nano*, 2020, **14**, 6812–6822.
107 N. Jiang, B. You, R. Boonstra, I. M. Terrero Rodriguez and Y. Sun, *ACS Energy Lett.*, 2016, **1**, 386–390.
108 Z. Zhou, C. Chen, M. Gao, B. Xia and J. Zhang, *Green Chem.*, 2019, **21**, 6699–6706.
109 M. J. Kang, H. J. Yu, H. S. Kim and H. G. Cha, *New J. Chem.*, 2020, **44**, 14239–14245.
110 R. Kumar, Z. Zhu, C. Chen, W. Cai, J. Woon-Chung Wong and J. Zhao, *ChemSusChem*, 2022, **15**, e202201333.
111 K. R. Vuyyuru and P. Strasser, *Catal. Today*, 2012, **195**, 144–154.
112 G. Yang, Y. Jiao, H. Yan, Y. Xie, A. Wu, X. Dong, D. Guo, C. Tian and H. Fu, *Adv. Mater.*, 2020, **32**, 2000455.
113 H. G. Cha and K.-S. Choi, *Nat. Chem.*, 2015, **7**, 328–333.
114 T. Cao, M. Wu, V. V. Ordomsky, X. Xin, H. Wang, P. Métivier and M. Pera-Titus, *ChemSusChem*, 2017, **10**, 4851–4854.
115 C. Lei, Z. Chen, T. Jiang, S. Wang, W. Du, S. Cha, Y. Hao, R. Wang, X. Cao and M. Gong, *Angew. Chem., Int. Ed.*, 2024, **63**, e202319642.
116 S. R. Kubota and K.-S. Choi, *ChemSusChem*, 2018, **11**, 2138–2145.
117 T. Wang, Y. Song, W. Zhao, C. Zhou, Y. Jin, X. Wan, Y. Dai and Y. Yang, *New J. Chem.*, 2021, **45**, 21285–21292.
118 M. P. J. M. van der Ham, E. van Keulen, M. T. M. Koper, A. A. Tashvigh and J. H. Bitter, *Angew. Chem., Int. Ed.*, 2023, **62**, e202306701.
119 T. Faverge, B. Gilles, A. Bonnefont, F. Maillard, C. Coutanceau and M. Chatenet, *ACS Catal.*, 2023, **13**, 2657–2669.
120 C.-C. Chen, C.-L. Lin and L.-C. Chen, *J. Power Sources*, 2015, **287**, 323–333.
121 J. Wang, J. Gong, Y. Xiong, J. Yang, Y. Gao, Y. Liu, X. Lu and Z. Tang, *Chem. Commun.*, 2011, **47**, 6894–6896.
122 A. Medrano-Banda, E. Ginoux, T. Faverge, A. Oshchepkov, A. Bonnefont, M. Chatenet, C. Coutanceau, G. Kéranguéven, P. Cognet and E. Savinova, *Electrochim. Acta*, 2024, **487**, 144159.
123 D. Bin, H. Wang, J. Li, H. Wang, Z. Yin, J. Kang, B. He and Z. Li, *Electrochim. Acta*, 2014, **130**, 170–178.
124 W.-J. Liu, Z. Xu, D. Zhao, X.-Q. Pan, H.-C. Li, X. Hu, Z.-Y. Fan, W.-K. Wang, G.-H. Zhao, S. Jin, G. W. Huber and H.-Q. Yu, *Nat. Commun.*, 2020, **11**, 265.
125 X. Lin, H. Zhong, W. Hu and J. Du, *Inorg. Chem.*, 2023, **62**, 10513–10521.
126 M. Tayebi, Z. Masoumi, B. Seo, C.-S. Lim, C. H. Hong, H. J. Kim, D. Kyung and H.-G. Kim, *ACS Appl. Mater. Interfaces*, 2024, **16**, 26107–26120.
127 S. Vogt, M. Schneider, H. Schäfer-Eberwein and G. Nöll, *Anal. Chem.*, 2014, **86**, 7530–7535.
128 M. P. J. M. van der Ham, J. Creus, J. H. Bitter, M. T. M. Koper and P. P. Pescarmona, *Chem. Rev.*, 2024, **124**, 11915–11961.
129 J. Luo and T. L. Liu, *J. Bioresour. Bioprod.*, 2023, **8**, 1–14.
130 J. González-Cobos, M. S. Prévot and P. Vernoux, *Curr. Opin. Electrochem.*, 2023, **39**, 101255.
131 M. Rafiee, M. Alherech, S. D. Karlen and S. S. Stahl, *J. Am. Chem. Soc.*, 2019, **141**, 15266–15276.
132 K. Beliaeva, M. Elsheref, D. Walden, F. Dappozze, A. Nieto-Marquez, S. Gil, C. Guillard, P. Vernoux, S. N. Steinmann and A. Caravaca, *J. Electrochem. Soc.*, 2020, **167**, 134511.
133 G. Liu, Z. Zhai, Y. Lu, J. Lu, Y. Wang, S. Liang, H. He and L. Jiang, *Chem Bio Eng.*, 2024, **1**, 357–365.
134 I. Bosque, G. Magallanes, M. Rigoulet, M. D. Kärkäs and C. R. J. Stephenson, *ACS Cent. Sci.*, 2017, **3**, 621–628.
135 A. Bailey and H. M. Brooks, *J. Am. Chem. Soc.*, 1946, **68**, 445–446.
136 C. Lan, H. Fan, Y. Shang, D. Shen and G. Li, *Sustainable Energy Fuels*, 2020, **4**, 1828–1836.
137 P. Parpot, A. P. Bettencourt, A. M. Carvalho and E. M. Belgsir, *J. Appl. Electrochem.*, 2000, **30**, 727–731.
138 M. Liu, Y. Wen, J. Qi, S. Zhang and G. Li, *ChemistrySelect*, 2017, **2**, 4956–4962.
139 P. Cai, H. Fan, S. Cao, J. Qi, S. Zhang and G. Li, *Electrochim. Acta*, 2018, **264**, 128–139.
140 R. Tolba, M. Tian, J. Wen, Z.-H. Jiang and A. Chen, *J. Electroanal. Chem.*, 2010, **649**, 9–15.
141 R. Ghahremani, F. Farales, F. Bateni and J. A. Staser, *J. Electrochem. Soc.*, 2020, **167**, 043502.
142 A. Caravaca, W. E. Garcia-Lorefice, S. Gil, A. De Lucas-Consuegra and P. Vernoux, *Electrochem. Commun.*, 2019, **100**, 43–47.
143 Y. Jia, Y. Wen, X. Han, J. Qi, Z. Liu, S. Zhang and G. Li, *Catal. Sci. Technol.*, 2018, **8**, 4665–4677.
144 S. Stiefel, J. Lölsberg, L. Kipshagen, R. Möller-Gulland and M. Wessling, *Electrochem. Commun.*, 2015, **61**, 49–52.
145 P. Hauke, S. Brückner and P. Strasser, *ACS Sustainable Chem. Eng.*, 2023, **11**, 13628–13635.
146 S.-Q. Liu, M.-R. Gao, S. Wu, R. Feng, Y. Wang, L. Cui, Y. Guo, X.-Z. Fu and J.-L. Luo, *Energy Environ. Sci.*, 2023, **16**, 5305–5314.
147 X. Liu, M. Albloushi, M. Galvin, C. W. Schroeder, Y. Wu and W. Li, *Green Chem.*, 2024, **26**, 11351–11363.
148 T. Rafaïdeen, S. Baranton and C. Coutanceau, *Appl. Catal., B*, 2019, **243**, 641–656.
149 T. Peng, T. Zhuang, Y. Yan, J. Qian, G. R. Dick, J. Behaghel De Bueren, S.-F. Hung, Y. Zhang, Z. Wang, J. Wicks, F. P. Garcia De Arquer, J. Abed, N. Wang, A. Sedighian Rasouli, G. Lee, M. Wang, D. He, Z. Wang, Z. Liang, L. Song, X. Wang, B. Chen, A. Ozden, Y. Lum, W. R. Leow, M. Luo, D. M. Meira, A. H. Ip, J. S. Luterbacher, W. Zhao and E. H. Sargent, *J. Am. Chem. Soc.*, 2021, **143**, 17226–17235.

150 S. Li, X. Sun, Z. Yao, X. Zhong, Y. Cao, Y. Liang, Z. Wei, S. Deng, G. Zhuang, X. Li and J. Wang, *Adv. Funct. Mater.*, 2019, **29**, 1904780.
151 F. Cui, S. Huang, R. Jin, H. Cui, X. Wu, Y. Dai, M. Guo and G. He, *Int. J. Hydrogen Energy*, 2022, **47**, 28086–28094.
152 T. Hibino, K. Kobayashi, M. Ito, M. Nagao, M. Fukui and S. Teranishi, *Appl. Catal., B*, 2018, **231**, 191–199.
153 R. Ghalta, A. Chauhan and R. Srivastava, *Sustainable Energy Fuels*, 2024, **8**, 3205–3246.
154 D. Aboagye, R. Djellabi, F. Medina and S. Contreras, *Angew. Chem., Int. Ed.*, 2023, **62**, e202301909.
155 X. Xu, L. Shi, S. Zhang, Z. Ao, J. Zhang, S. Wang and H. Sun, *Chem. Eng. J.*, 2023, **469**, 143972.
156 N. Luo, M. Wang, H. Li, J. Zhang, H. Liu and F. Wang, *ACS Catal.*, 2016, **6**, 7716–7721.
157 N. Luo, M. Wang, H. Li, J. Zhang, T. Hou, H. Chen, X. Zhang, J. Lu and F. Wang, *ACS Catal.*, 2017, **7**, 4571–4580.
158 X. Wu, X. Fan, S. Xie, J. Lin, J. Cheng, Q. Zhang, L. Chen and Y. Wang, *Nat. Catal.*, 2018, **1**, 772–780.
159 G. Han, T. Yan, W. Zhang, Y. C. Zhang, D. Y. Lee, Z. Cao and Y. Sun, *ACS Catal.*, 2019, **9**, 11341–11349.
160 H. Yoo, M.-W. Lee, S. Lee, J. Lee, S. Cho, H. Lee, H. G. Cha and H. S. Kim, *ACS Catal.*, 2020, **10**, 8465–8475.
161 D. Dai, J. Qiu, G. Xia, Y. Tang and J. Yao, *ACS Catal.*, 2023, **13**, 14987–14995.
162 R. Ghalta and R. Srivastava, *Green Chem.*, 2024, **26**, 7384–7405.
163 Z. Peng, Z. Wu, X. Sun and H. Li, *Green Chem.*, 2023, **25**, 6869–6880.
164 D. W. Wakerley, M. F. Kuehnel, K. L. Orchard, K. H. Ly, T. E. Rosser and E. Reisner, *Nat. Energy*, 2017, **2**, 17021.
165 A. Speltini, M. Sturini, D. Dondi, E. Annovazzi, F. Maraschi, V. Caratto, A. Profumo and A. Buttafava, *Photochem. Photobiol. Sci.*, 2014, **13**, 1410–1419.
166 A. Caravaca, W. Jones, C. Hardacre and M. Bowker, *Proc. R. Soc. London, Ser. A*, 2016, **472**, 20160054.
167 T. Kawai and T. Sakata, *Nature*, 1980, **286**, 474–476.
168 H. Hao, L. Zhang, W. Wang and S. Zeng, *ChemSusChem*, 2018, **11**, 2810–2817.
169 L. Wang, Z. Zhang, L. Zhang, S. Xue, W. O. S. Doherty, I. M. O'Hara and X. Ke, *RSC Adv.*, 2015, **5**, 85242–85247.
170 C. Li, J. Li, L. Qin, P. Yang and D. G. Vlachos, *ACS Catal.*, 2021, **11**, 11336–11359.
171 Q. Zhang, B. Gu and W. Fang, *Green Chem.*, 2024, **26**, 6261–6288.
172 G. C. de Assis, I. M. A. Silva, T. G. dos Santos, T. V. dos Santos, M. R. Meneghetti and S. M. P. Meneghetti, *Catal. Sci. Technol.*, 2021, **11**, 2354–2360.
173 S. Chu, J. Shao, H. Qu, X. Wang, R. Xiao and H. Zhang, *ChemSusChem*, 2023, **16**, e202300886.
174 J. Zhao, Y. Wang, H. Liu, R. Zhang, W. Jia, J. Zhang, Y. Sun and L. Peng, *ACS Catal.*, 2025, **15**, 3464–3474.
175 Y. An, T. Lei, W. Jiang and H. Pang, *Green Chem.*, 2024, **26**, 10739–10773.
176 T. Hang, L. Wu, W. Liu, L. Yang and T. Zhang, *Adv. Energy Sustainability Res.*, 2024, **5**, 2400069.
177 C. Jin, M. Han, Y. Wu and S. Wang, *Energy Environ. Sci.*, 2024, **17**, 7459–7511.
178 D. Tang, J. Liu, X. Zhang, L. Chen, L. Ma and Q. Zhang, *Green Chem.*, 2023, **25**, 7843–7862.
179 X. Liu, W. Wei and B.-J. Ni, in *Solar-to-Chemical Conversion*, John Wiley & Sons, Ltd, 2021, pp. 389–417.
180 M. G. Sendeku, T. A. Shifa, F. T. Dajan, K. B. Ibrahim, B. Wu, Y. Yang, E. Moretti, A. Vomiero and F. Wang, *Adv. Mater.*, 2024, **36**, 2308101.
181 Y. Kageshima, T. Yoshimura, S. Koh, M. Mizuno, K. Teshima and H. Nishikiori, *ChemCatChem*, 2021, **13**, 1530–1537.
182 Y. Kageshima, H. Wada, K. Teshima and H. Nishikiori, *Appl. Catal., B*, 2023, **327**, 122431.
183 N. Le Duy, P.-C. Chuang, C.-Y. Lin and Y.-H. Lai, *J. Photochem. Photobiol., A*, 2025, **458**, 115932.
184 K. Jakubow-Piotrowska, B. Witkowski and J. Augustynski, *Commun. Chem.*, 2022, **5**, 1–10.
185 S. Bhattacharjee, V. Andrei, C. Pornrungroj, M. Rahaman, C. M. Pichler and E. Reisner, *Adv. Funct. Mater.*, 2022, **32**, 2109313.
186 C. R. Lhermitte, N. Plainpan, P. Canjura, F. Boudoire and K. Sivula, *RSC Adv.*, 2021, **11**, 198–202.
187 J. J. Roylance, T. W. Kim and K.-S. Choi, *ACS Catal.*, 2016, **6**, 1840–1847.
188 H. Zhang, S. Li, J. Xu, C. Ru, J. Yu, J. Luo, L. Mu, W. Shi and G. She, *Chem. – Asian J.*, 2025, **20**, e202401284.
189 S. K. Pahari and Y.-T. Chen, *Chem. Eng. J.*, 2023, **473**, 145232.
190 B. Liu, Y. Qi, X. Qiu, H. Zou, X. Lin and Y. Qin, *Adv. Funct. Mater.*, 2025, 2421552.
191 J. Kim, Y. Um, S. Han, T. Hilberath, Y. H. Kim, F. Hollmann and C. B. Park, *ACS Appl. Mater. Interfaces*, 2022, **14**, 11465–11473.
192 D. Wang, S. H. Lee, S. Han, J. Kim, N. V. T. Trang, K. Kim, E.-G. Choi, P. Boonmongkolras, Y. W. Lee, B. Shin, Y. H. Kim and C. B. Park, *Green Chem.*, 2020, **22**, 5151–5160.
193 Y. Choi, R. Mehrotra, S.-H. Lee, T. V. T. Nguyen, I. Lee, J. Kim, H.-Y. Yang, H. Oh, H. Kim, J.-W. Lee, Y. H. Kim, S.-Y. Jang, J.-W. Jang and J. Ryu, *Nat. Commun.*, 2022, **13**, 5709.
194 D. V. Esposito, R. V. Forest, Y. Chang, N. Gaillard, B. E. McCandless, S. Hou, K. H. Lee, R. W. Birkmire and J. G. Chen, *Energy Environ. Sci.*, 2012, **5**, 9091–9099.
195 P.-C. Chuang, C.-Y. Lin, S.-T. Ye and Y.-H. Lai, *Small*, 2024, **20**, 2404478.
196 R. M. Fabrao, J. F. de Brito, J. L. da Silva, N. R. Stradiotto and M. V. B. Zanoni, *Electrochim. Acta*, 2016, **222**, 123–132.
197 Z. Tian, Y. Da, M. Wang, X. Dou, X. Cui, J. Chen, R. Jiang, S. Xi, B. Cui, Y. Luo, H. Yang, Y. Long, Y. Xiao and W. Chen, *Nat. Commun.*, 2023, **14**, 142.
198 P.-C. Chuang and Y.-H. Lai, *Catal. Sci. Technol.*, 2022, **12**, 6375–6383.
199 L. Özcan, P. Yalçın, O. Alagöz and S. Yurdakal, *Catal. Today*, 2017, **281**, 205–213.

200 L. Zheng, P. Xu, Y. Zhao, Z. Bao, X. Luo, X. Shi, Q. Wu and H. Zheng, *Appl. Catal., B*, 2023, **331**, 122679.
201 D. J. Chadderdon, L.-P. Wu, Z. A. McGraw, M. Panthani and W. Li, *ChemElectroChem*, 2019, **6**, 3387–3392.
202 A. Kawde, M. Sayed, Q. Shi, J. Uhlig, T. Pullerits and R. Hatti-Kaul, *Catalysts*, 2021, **11**, 969.
203 I. Carrai, R. Mazzaro, E. Bassan, G. Morselli, A. Piccioni, S. Grandi, S. Caramori, P. Ceroni and L. Pasquini, *Sol. RRL*, 2023, **7**, 2300205.
204 E. Marchini, S. Carli, D. Barboni, M. Catani, A. Cavazzini, S. Caramori and S. Berardi, *ChemSusChem*, 2024, e202401782.
205 R. Pelegrini, J. Reyes, N. Durán, P. P. Zamora and A. R. de Andrade, *J. Appl. Electrochem.*, 2000, **30**, 953–958.
206 M. Tian, J. Wen, D. MacDonald, R. M. Asmussen and A. Chen, *Electrochem. Commun.*, 2010, **12**, 527–530.
207 J. King and S. S. C. Chuang, *Catal. Commun.*, 2021, **149**, 106219.
208 T. Li, J. Y. Mo, D. M. Weekes, K. E. Dettelbach, R. P. Jansonius, G. M. Sammis and C. P. Berlinguette, *ChemSusChem*, 2020, **13**, 3622–3626.
209 P. Wu, L. Li, H. Li and Z. Fang, *Chem. Eng. J.*, 2024, **490**, 151722.
210 S. Li, Z.-J. Li, H. Yu, M. R. Sytu, Y. Wang, D. Beeri, W. Zheng, B. D. Sherman, C. G. Yoo and G. Leem, *ACS Energy Lett.*, 2020, **5**, 777–784.
211 S. Li, E. W. Shuler, D. Willinger, H. T. Nguyen, S. Kim, H. C. Kang, J.-J. Lee, W. Zheng, C. G. Yoo, B. D. Sherman and G. Leem, *ACS Appl. Mater. Interfaces*, 2022, **14**, 22799–22809.
212 S. Li, S. Kim, A. H. Davis, J. Zhuang, E. W. Shuler, D. Willinger, J.-J. Lee, W. Zheng, B. D. Sherman, C. G. Yoo and G. Leem, *ACS Catal.*, 2021, **11**, 3771–3781.
213 Y. Pan, H. Zhang, B. Zhang, F. Gong, J. Feng, H. Huang, S. Vanka, R. Fan, Q. Cao, M. Shen, Z. Li, Z. Zou, R. Xiao and S. Chu, *Nat. Commun.*, 2023, **14**, 1013.
214 H. Chen, C. Ding, Y. Li, L. Wang, C. Li and J. He, *J. Environ. Chem. Eng.*, 2024, **12**, 112614.
215 N. M. Haegel, H. Atwater, T. Barnes, C. Breyer, A. Burrell, Y.-M. Chiang, S. De Wolf, B. Dimmler, D. Feldman, S. Glunz, J. C. Goldschmidt, D. Hochschild, R. Inzunza, I. Kaizuka, B. Kroposki, S. Kurtz, S. Leu, R. Margolis, K. Matsubara, A. Metz, W. K. Metzger, M. Morjaria, S. Niki, S. Nowak, I. M. Peters, S. Philipps, T. Reindl, A. Richter, D. Rose, K. Sakurai, R. Schlatmann, M. Shikano, W. Sinke, R. Sinton, B. J. Stanbery, M. Topic, W. Tumas, Y. Ueda, J. van de Lagemaat, P. Verlinden, M. Vetter, E. Warren, M. Werner, M. Yamaguchi and A. W. Bett, *Science*, 2019, **364**, 836–838.
216 M. Woodhouse, D. Feldman, V. Ramasamy, B. Smith, T. Silverman, T. Barnes, J. Zuboy and R. Margolis, *Research and Development Priorities to Advance Solar Photovoltaic Lifecycle Costs and Performance*, 2021.
217 K. J. Zeitsch, *The chemistry and technology of furfural and its many by-products*, Elsevier, Amsterdam, New York, 2000.
218 J.-P. Lange, E. van der Heide, J. van Buijtenen and R. Price, *ChemSusChem*, 2012, **5**, 150–166.
219 A. Racha, C. Samanta, S. Sreekantan and B. Marimuthu, *Energy Fuels*, 2023, **37**, 11475–11496.
220 G. Lopez, D. Keiner, M. Fasihi, T. Koiranen and C. Breyer, *Energy Environ. Sci.*, 2023, **16**, 2879–2909.
221 F. Brissaud, A. Chaise, K. Gault and S. Soual, *Int. J. Hydrogen Energy*, 2024, **49**, 925–932.
222 M. Genovese, D. Blekhman, M. Dray and P. Fragiacomo, *Int. J. Hydrogen Energy*, 2024, **52**, 688–704.
223 V. N. Emel'yanenko, A. Dabrowska, S. P. Verevkin, M. O. Hertel, H. Scheuren and K. Sommer, *J. Chem. Eng. Data*, 2007, **52**, 468–471.
224 G. Fraga, J. Ramirez, M. Renouf and N. Batalha, *ACS Sustainable Chem. Eng.*, 2024, **12**, 10604–10614.
225 M. Jiang, J. Tan, Y. Chen, W. Zhang, P. Chen, Y. Tang and Q. Gao, *Chem. Commun.*, 2023, **59**, 3103–3106.
226 D. Jin, A. Chen and B.-L. Lin, *J. Am. Chem. Soc.*, 2024, jacs.4c02754.
227 A. J. Bard, L. R. Faulkner, C. G. Zoski and J. Leddy, *Electrochemical methods: fundamentals and applications*, John Wiley, New York, 2nd edn, 2001.
228 T. Shinagawa, A. T. Garcia-Esparza and K. Takanabe, *Sci. Rep.*, 2015, **5**, 13801.
229 R. G. Grim, J. R. F. Iii, Z. Huang, L. Tao and M. G. Resch, *Joule*, 2023, **7**, 1684–1699.
230 Hydrogen Europe, 2024.
231 Q. Li, T. U. Rao, Y. Uehara, H. Machida, Z. Huo and K. Norinaga, *ACS Sustainable Resour. Manage.*, 2024, **1**, 316–327.
232 N. Viar, I. Agirre and I. Gandarias, *Chem. Eng. J.*, 2024, **480**, 147873.
233 B.-H. Zhao, F. Chen, M. Wang, C. Cheng, Y. Wu, C. Liu, Y. Yu and B. Zhang, *Nat. Sustainable*, 2023, **6**, 827–837.
234 M. W. Schreiber, *Curr. Opin. Electrochem.*, 2023, 101438.
235 J.-P. Lange, *Catal. Today*, 2024, **435**, 114726.
236 A. Hofrichter, D. Rank, M. Heberl and M. Sterner, *Int. J. Hydrogen Energy*, 2023, **48**, 1651–1663.
237 F. Radner, N. Strobl, M. Köberl, J. Rauh, K. Esser, F. Winkler and A. Trattner, *Energy Convers. Manage.: X*, 2023, **20**, 100502.
238 J. Eichman, M. Koleva, O. J. Guerra and B. McLaughlin, *Optimizing an Integrated Renewable-Electrolysis System*, 2020.
239 Frequently Asked Questions (FAQs) – U.S. Energy Information Administration (EIA), https://www.eia.gov/tools/faqs/faq.php, (accessed January 12, 2025).
240 E. Nguyen, P. Olivier, M.-C. Pera, E. Pahon and R. Roche, *Int. J. Hydrogen Energy*, 2024, **70**, 474–492.
241 H. Kojima, K. Nagasawa, N. Todoroki, Y. Ito, T. Matsui and R. Nakajima, *Int. J. Hydrogen Energy*, 2023, **48**, 4572–4593.
242 D. Virah-Sawmy, F. J. Beck and B. Sturmberg, *Int. J. Hydrogen Energy*, 2024, **72**, 49–59.
243 C. Gollier, *J. Environ. Econ. Manage.*, 2024, **128**, 103062.
244 R. T. Shafiee and D. P. Schrag, *Joule*, 2024, **8**, 3281–3289.
245 Y. Liu, B. Zhong and A. Lawal, *RSC Adv.*, 2022, **12**, 27997–28008.
246 A. J. J. E. Eerhart, M. K. Patel and A. P. C. Faaij, *Biofuels, Bioprod. Biorefin.*, 2015, **9**, 307–325.

247 A. J. J. E. Eerhart, A. P. C. Faaij and M. K. Patel, *Energy Environ. Sci.*, 2012, **5**, 6407–6422.
248 Life Cycle Assessment study demonstrates the potential of Avantium's FDCA and PEF technology to curb global warming, https://newsroom.avantium.com/life-cycle-assessment-study-demonstrates-the-potential-of-avantiums-fdca-and-pef-technology-to-curb-global-warming/, (accessed February 3, 2025).
249 R. Lin, H. Yang, H. Zheng, M. Salehi, A. Farzi, P. Patel, X. Wang, J. Guo, K. Liu, Z. Gao, X. Li and A. Seifitokaldani, *RSC Sustainability*, 2024, **2**, 445–458.
250 T. Moore, D. I. Oyarzun, W. Li, T. Y. Lin, M. Goldman, A. A. Wong, S. A. Jaffer, A. Sarkar, S. E. Baker, E. B. Duoss and C. Hahn, *Joule*, 2023, **7**, 782–796.
251 P. J. L. Broersen, J. J. N. Koning, G. Rothenberg and A. C. Garcia, *ChemSusChem*, 2024, **17**, e202400582.
252 F. Schwarz, E. Larenz and A. K. Mechler, *Green Chem.*, 2024, **26**, 4645–4652.
253 Z. Li, Y. Yan, S.-M. Xu, H. Zhou, M. Xu, L. Ma, M. Shao, X. Kong, B. Wang, L. Zheng and H. Duan, *Nat. Commun.*, 2022, **13**, 147.
254 Y. Wu, X. Zhu, S. Du, G. Huang, B. Zhou, Y. Lu, Y. Li, S. P. Jiang, L. Tao and S. Wang, *Proc. Natl. Acad. Sci. U. S. A.*, 2023, **120**, e2300625120.
255 J. A. Muldoon and B. G. Harvey, *ChemSusChem*, 2020, **13**, 5777–5807.
256 M. L. Stone, M. S. Webber, W. P. Mounfield, D. C. Bell, E. Christensen, A. R. C. Morais, Y. Li, E. M. Anderson, J. S. Heyne, G. T. Beckham and Y. Román-Leshkov, *Joule*, 2022, **6**, 2324–2337.
257 M. S. Webber, J. Watson, J. Zhu, J. H. Jang, M. Çağlayan, J. S. Heyne, G. T. Beckham and Y. Román-Leshkov, *Nat. Mater.*, 2024, **23**, 1622–1638.
258 H. Zhou, Y. Ren, B. Yao, Z. Li, M. Xu, L. Ma, X. Kong, L. Zheng, M. Shao and H. Duan, *Nat. Commun.*, 2023, **14**, 5621.
259 R. Stanger, T. Wall, R. Spörl, M. Paneru, S. Grathwohl, M. Weidmann, G. Scheffknecht, D. McDonald, K. Myöhänen, J. Ritvanen, S. Rahiala, T. Hyppänen, J. Mletzko, A. Kather and S. Santos, *Int. J. Greenhouse Gas Control*, 2015, **40**, 55–125.
260 Y. Lum, J. E. Huang, Z. Wang, M. Luo, D.-H. Nam, W. R. Leow, B. Chen, J. Wicks, Y. C. Li, Y. Wang, C.-T. Dinh, J. Li, T.-T. Zhuang, F. Li, T.-K. Sham, D. Sinton and E. H. Sargent, *Nat. Catal.*, 2020, **3**, 14–22.
261 J. Yu, C. B. I. Musgrave, Q. Chen, Y. Yang, C. Tian, X. Hu, G. Su, H. Shin, W. Ni, X. Chen, P. Ou, Y. Liu, N. M. Schweitzer, D. M. Meira, V. P. Dravid, W. A. I. Goddard, K. Xie and E. H. Sargent, *J. Am. Chem. Soc.*, 2024, **146**, 32660–32669.
262 W. R. Leow, Y. Lum, A. Ozden, Y. Wang, D.-H. Nam, B. Chen, J. Wicks, T.-T. Zhuang, F. Li, D. Sinton and E. H. Sargent, *Science*, 2020, **368**, 1228–1233.
263 J.-G. Rosenboom, D. K. Hohl, P. Fleckenstein, G. Storti and M. Morbidelli, *Nat. Commun.*, 2018, **9**, 2701.
264 J. Sisler, S. Khan, A. H. Ip, M. W. Schreiber, S. A. Jaffer, E. R. Bobicki, C.-T. Dinh and E. H. Sargent, *ACS Energy Lett.*, 2021, **6**, 997–1002.
265 A. J. J. E. Eerhart, W. J. J. Huijgen, R. J. H. Grisel, J. C. van der Waal, E. de Jong, A. de S. Dias, A. P. C. Faaij and M. K. Patel, *RSC Adv.*, 2013, **4**, 3536–3549.
266 T. Alerte, A. Gaona, J. P. Edwards, C. M. Gabardo, C. P. O'Brien, J. Wicks, L. Bonnenfant, A. S. Rasouli, D. Young, J. Abed, L. Kershaw, Y. C. Xiao, A. Sarkar, S. A. Jaffer, M. W. Schreiber, D. Sinton, H. L. MacLean and E. H. Sargent, *ACS Sustainable Chem. Eng.*, 2023, **11**, 15651–15662.
267 Y. Ren, W. Kong, Y. Li, W. Zhan, C. Zhang, Y. Miao, B. Yao, S. Li, Z. Li, X. Liu, S. Zhan, H. Zhou, M. Shao and H. Duan, *Nat. Catal.*, 2025, DOI: 10.1038/s41929-025-01374-x.